Progress in Neurobiology 216 (2022) 102288

Contents lists available at ScienceDirect

Progress in Neurobiology

journal homepage: www.elsevier.com/locate/pneurobio

Original research article

Brain Dp140 alters glutamatergic transmission and social behaviour in the *mdx52* mouse model of Duchenne muscular dystrophy

Yasumasa Hashimoto [a,b,c], Hiroshi Kuniishi [d,e], Kazuhisa Sakai [f], Yuta Fukushima [g], Xuan Du [g], Kunihiko Yamashiro [h], Kei Hori [h], Michihiro Imamura [a], Mikio Hoshino [b,h], Mitsuhiko Yamada [e], Toshiyuki Araki [i], Hiroyuki Sakagami [j], Shin'ichi Takeda [a], Keiji Itaka [g], Noritaka Ichinohe [f], Francesco Muntoni [k], Masayuki Sekiguchi [d,*], Yoshitsugu Aoki [a,b,**]

[a] *Department of Molecular Therapy, National Institute of Neuroscience, National Center of Neurology and Psychiatry (NCNP), Kodaira, Tokyo 187-8502, Japan*
[b] *Department of NCNP Brain Physiology and Pathology, Graduate school of Medical and Dental Sciences, Tokyo Medical and Dental University (TMDU), Bunkyo, Tokyo 113-8510 Japan*
[c] *Department of Neurology, Kansai Medical University, Osaka 573-1010, Japan*
[d] *Department of Degenerative Neurological Diseases, National Institute of Neuroscience, NCNP, Kodaira, Tokyo 187-8502, Japan*
[e] *Department of Neuropsychopharmacology, National Institute of Mental Health, NCNP, Kodaira, Tokyo 187-8502, Japan*
[f] *Department of Ultrastructural Research, National Institute of Neuroscience, NCNP, Kodaira, Tokyo 187-8502, Japan*
[g] *Department of Biofunction Research, Institute of Biomaterials and Bioengineering, Tokyo Medical and Dental University (TMDU), Chiyoda, Tokyo 101-0062 Japan*
[h] *Department of Biochemistry and Cellular Biology, National Institute of Neuroscience, NCNP, Kodaira, Tokyo 187-8502, Japan*
[i] *Department of Peripheral Nervous System Research, National Institute of Neuroscience, NCNP, Kodaira, Tokyo 187-8502, Japan*
[j] *Department of Anatomy, Kitasato University School of Medicine, Sagamihara, Kanagawa 252-0374, Japan*
[k] *Dubowitz Neuromuscular Centre, NIHR Great Ormond Street Hospital Biomedical Research Centre, Great Ormond Street Institute of Child Health, University College London, & Great Ormond Street Hospital Trust, 30 Guilford Street, London, UK*

A R T I C L E I N F O

Keywords:
Duchenne muscular dystrophy (DMD)
Dystrophin protein (Dp) isoforms
Dp140
Basolateral amygdala (BLA)
Neurotransmission
RNA therapy

A B S T R A C T

Duchenne muscular dystrophy (DMD) is a muscle disorder caused by *DMD* mutations and is characterized by neurobehavioural comorbidities due to dystrophin deficiency in the brain. The lack of Dp140, a dystrophin short isoform, is clinically associated with intellectual disability and autism spectrum disorders (ASDs), but its postnatal functional role is not well understood. To investigate synaptic function in the presence or absence of brain Dp140, we utilized two DMD mouse models, *mdx23* and *mdx52* mice, in which Dp140 is preserved or lacking, respectively. ASD-like behaviours were observed in pups and 8-week-old *mdx52* mice lacking Dp140. Paired-pulse ratio of excitatory postsynaptic currents, glutamatergic vesicle number in basolateral amygdala neurons, and glutamatergic transmission in medial prefrontal cortex-basolateral amygdala projections were significantly reduced in *mdx52* mice compared to those in wild-type and *mdx23* mice. ASD-like behaviour and electrophysiological findings in *mdx52* mice were ameliorated by restoration of Dp140 following intra-cerebroventricular injection of antisense oligonucleotide drug-induced exon 53 skipping or intra-basolateral amygdala administration of *Dp140* mRNA-based drug. Our results implicate Dp140 in ASD-like behaviour via altered glutamatergic transmission in the basolateral amygdala of *mdx52* mice.

Abbreviations: DMD, Duchenne muscular dystrophy; Dp-, -kDa dystrophin protein; ASDs, autism spectrum disorders; ADHD, attention-deficit/hyperactivity disorder; WT, wild-type; BLA, basolateral amygdala; mPFC, medial prefrontal cortex; E-I balance, excitatory-inhibitory balance; EPSC, excitatory postsynaptic current; IPSC, inhibitory postsynaptic current; mEPSCs, miniature excitatory postsynaptic currents; mIPSCs, miniature inhibitory postsynaptic currents; AAV5-CaMKIIa-ChR2-EYFP, Serotype 5 adeno-associated virus expression of channelrhodopsin-2 fused to an enhanced yellow fluorescent protein driven by alpha-Calcium/calmodulin-dependent kinase II promoter; VGLUT, vesicular glutamate transporters; PSD, postsynaptic density; ASO, antisense oligonucleotide.

* Corresponding author.
** Corresponding author at: Department of Molecular Therapy, National Institute of Neuroscience, National Center of Neurology and Psychiatry (NCNP), Kodaira, Tokyo 187-8502, Japan.
E-mail addresses: sekiguch@ncnp.go.jp (M. Sekiguchi), tsugu56@ncnp.go.jp (Y. Aoki).

https://doi.org/10.1016/j.pneurobio.2022.102288
Received 19 April 2021; Received in revised form 6 April 2022; Accepted 25 May 2022
Available online 30 May 2022

1. Introduction

Duchenne muscular dystrophy (DMD) is an X-linked disorder caused by nonsense and frameshift mutations in the *DMD* gene (Hoffman et al., 1987). DMD is characterized by cognitive impairments and behavioural problems alongside skeletal muscle disorder in approximately 30 % of DMD patients (Bresolin et al., 1994; Motulsky, 1987; Wicksell et al., 2004). The incidence of psychiatric symptoms such as intellectual disability, autism spectrum disorder (ASD) (Fujino et al., 2018; Hinton et al., 2009; Komoto et al., 1984), attention-deficit/hyperactivity disorder (ADHD) (Hendriksen and Vles, 2008; Pane et al., 2012), and anxiety disorder (Filippo et al., 2012; Roccella et al., 2003) is higher in DMD patients. Further, emotional responses such as fear and stress are associated with the *DMD* gene (Frésard et al., 2012; Nonneman et al., 2012; Razzoli et al., 2020).

The *DMD* gene is highly expressed in the adult human amygdala and hippocampus (Doorenweerd et al., 2017). Tissue-specific promoters of the *DMD* and the *Dmd* gene give rise to different dystrophin protein isoforms. Each dystrophin isoform, including full-length dystrophin protein Dp427, brain-specific Dp140, and ubiquitous Dp71, is regulated by independent promoters in the human and murine brain (Supplementary Fig. 1A) (Lidov et al., 1990; Muntoni et al., 2003). Dp427 forms a dystrophin-glycoprotein complex at GABAergic postsynapses of pyramidal neurons and regulates $GABA_A$ receptor clustering (Knuesel et al., 1999; Waite et al., 2012), whereas Dp140 is highly expressed throughout the central nervous system, including the amygdala, from the foetal period to infancy. Based on gene ontology analysis, Dp140 is associated with genes involved in early neurodevelopment (Doorenweerd et al., 2017). Notably, exacerbation of cognitive impairments in human DMD is linked to distal *DMD* mutations affecting brain-specific Dp140 expression, which derives from a brain-specific promoter located in intron 44, with its translation start site in exon 51, and a 5'UTR composed of the Dp427 exons 45–50 in the DMD gene (Bardoni et al., 2000a, 2000b; Chamova et al., 2013; Felisari et al., 2000). Regarding neurobehavioural comorbidities, we previously reported that compared with DMD patients affecting only the Dp427, those with mutations also affecting the shorter dystrophin isoform were more than twice as likely to have a clustering of psychiatric symptoms (Ricotti et al., 2016).

We previously reported that in the *mdx* mice lacking Dp427 in the muscle and the brain, the $GABA_A$ receptor subunit cluster number in the basolateral amygdala (BLA) was reduced, resulting in impaired amygdala GABAergic transmission and enhanced defensive behaviour (Sekiguchi et al., 2009). However, the detailed molecular functions of Dp140 in the murine amygdala are not well understood, and Dp140-specific knockout mouse does not exist. Here, we utilized two different dystrophic mouse models, namely the commonly studied *mdx* (referred to as *mdx23* in our study) and *mdx52* mice, to clarify brain-specific molecular functions of Dp140. The *mdx23* mouse line has a nonsense mutation in *Dmd* exon 23, resulting in a lack of Dp427. In contrast, the *mdx52* mouse line has a deletion of *Dmd* exon 52 (Araki et al., 1997a, 1997b), resulting in a lack of both Dp140 and Dp427 (Supplementary Fig. 1A-C). Therefore, we hypothesized that the lack of Dp140 in addition to Dp427 might exacerbate ASD-like behaviours and alter GABAergic and glutamatergic transmission in *mdx52* mice compared with *mdx23* mice.

2. Methods and materials

2.1. Animals

As the *Dmd* gene is located on chromosome X in the mouse, male *mdx23* mice, *mdx52* mice (Araki et al., 1997a, 1997b), and their wild-type (WT) littermates were obtained by mating a dystrophin heterozygote female (+/-) with a male WT mouse (C57BL/6 J) (genotype at random). C57BL/6-background *mdx23* mice were generously given by Dr. Sasaoka (Niigata University) and maintained in our animal facility (Nogami et al., 2021). The heterozygote female used was obtained by mating three pairs of male WT mice and homozygote female *mdx23* or *mdx52* (C57BL/6 J *mdx23* or *mdx52*) mice, both of which were maintained in our facility. Littermate pairs were used in behavioural tests. A tail sample was excised for genotyping after behavioural tests. Genotyping was performed using previously described PCR methods. Thus, experimenters were blind to genotype in behavioural tests. Throughout experiments, including examination of developmental changes in the sensitivity to restraint, each male mouse was used for one test only, and repetitive uses in other tests were avoided. Animal care was provided by the Animal Center in the National Center of Neurology and Psychiatry. These mice were housed four or five per cage (15 ×22 x 12 cm) under controlled conditions of temperature (25 ± 1 ℃), reared in normal lighting conditions (12-h light/dark cycle), and provided with food and water ad libitum. All behavioural experiments were performed between 9 am and 3 pm in strict accordance with the regulations of the National Institute of Neuroscience and the National Center of Neurology and Psychiatry (Japan) for animal experiments and were approved by the Animal Investigation Committee of the Institute (Approval number: 2019012). All efforts were made to minimize both suffering and the number of animals used.

2.2. Behavioural test-1 "social behaviour"

Social interaction test was applied to the previous apparatus (Makinodan et al., 2012) in 8-week-old male mice. Two metallic perforated boxes (7 ×7 x 11 cm), one of which contained a male WT mouse at 8 weeks of age, were placed in the open field arena (50 ×50 x 40 cm, O'Hara & Co., Ltd., Tokyo, Japan) after the open field test as indicated by Behavioural test-4 as habituation to the test apparatus. The experimental mouse at 8 weeks of age was placed in the arena and allowed to freely explore the field and the two boxes for 10 min. The interaction time was recorded when the nose of the subjected mouse was directly contacted (sniffing and touching) to each of the boxes.

2.3. Behavioural test-2 "ultrasonic vocalizations for communications"

The male pups (P7) were individually housed with an UltraSoundGate system (Avisoft bioacoustics, Glienicke, Germany) composed of a CM16/CMPA condenser microphone, Avisoft-UltraSoundGate 116 H computer interface, and Avisoft Recorder software with a sampling rate of 400 kHz as described previously (Hori et al., 2020). A microphone was hung 16 cm above the floor of a soundproof box. On the day of the study, the pups with their mother were moved to the experimental room at least 30 min before the initiation of the study. After habituation, each pup was removed from its mother and placed on a 9 cm dish in the soundproof box. After the number of vocalizations was measured for 3 min, the pups were returned to their mother. Vocal signals recorded in wav files were automatically detected by MATLAB-based software USVSEG with modification to mouse USVs (Tachibana et al., 2014). This software segments each syllable and exports it as individual jpeg files. The number of USVs and the duration of each call are automatically detected. By observing jpeg files, experimenters manually excluded the files of vocalizations that include only click-like sounds without any tone-like signals, or that could not be classified into any call types as noises (false positive).

2.4. Behavioural test-3 "freezing response"

Restraint-induced and electrical foot-shock-induced freezing tests were performed as described previously (Sekiguchi et al., 2009), and the detail is described in Supplementary Information.

2.5. Behavioural test-4 "anxiety-like and self-grooming behaviours"

Open-field tests were performed in an arena (50 ×50 x 40 cm,

O'Hara & Co., Ltd., Tokyo, Japan) that was placed in the same sound-proof box as described previously (Kuniishi et al., 2020). Eight-week-old male mice were placed at the periphery of the arena, and the behaviour of mice for 10 min was recorded by a software-driven automated system (TimeOFCR1, O'Hara & Co., Ltd). The light intensity was 80 lx at the center of the arena. Their time in the center area (30 ×30 cm), their walking speeds, and their total distances were quantitated using a software-driven automated system (TimeOFCR1, O'Hara & Co., Ltd). The self-grooming behaviour during this test was examined. The apparatus was cleaned with 70 % ethanol before each test.

2.6. Electrophysiology

Each 8-week-old male mouse was anesthetized with halothane, and the brain was removed quickly in less than 1 min without damaging the cerebral base using fine super-cut scissors and round-tip forceps. Whole-cell patch-clamp recording from pyramidal neurons in the basolateral amygdala was performed as previously described (Sekiguchi et al., 2009). Brain slices (300 μm thick) containing the amygdala were prepared in artificial cerebrospinal fluid (ACSF; containing [in mM] 125 NaCl, 4.4 KCl, 1.5 $MgSO_4$, 1.0 NaH_2PO_4, 26 $NaHCO_3$, 10 glucose, 2.5 $CaCl_2$), pH 7.4, 290–300 mOsm /L) using a vibratome (Vibratome 3000). The slices were maintained for at least 30 min at room temperature in ACSF and continuously bubbled with 95 % O_2 /5 % CO_2. Brain slices were perfused (3.0 ml/min, gravity flow) with ACSF maintained at 28–32 °C with an in-line heater and an automatic temperature controller (Warner Instruments, Hamden, CT, USA). Patch electrodes (resistance 4–7 MΩ) were filled with a solution containing the following: (in mM) 100 $CsMeSO_4$, 15.5 CsCl, 10 HEPES, 0.25 EGTA, 10 glucose, 0.3 Na_3GTP, 2 MgATP, 3 QX-314, 48.5 Sucrose, pH 7.25 with NaOH, 280–290 mOsM. The electrophysiological signal was amplified and filtered at 5 kHz using a MultiClamp 700B patch-clamp amplifier (Axon Instruments, Union City, CA, USA). Data were digitized at 50 kHz and acquired using Clampex software (version10.6, Axon Instruments). The access resistance, which was frequently checked during recording, was between 10 and 25 MΩ. Cells with large drifts (± 20%) in resistance were excluded from the analysis. Patch-clamp recordings were taken from pyramidal-shaped principal neurons. Between 1 and 4 basolateral amygdala (BLA) pyramidal neurons were assessed in each brain slice, 3 brain slices were obtained from a mouse, and 4–6 mice per group were used. Synaptic responses obtained by electrical stimulation were elicited with a stimulating bipolar electrode (CBABD50, FHC, Bowdoin, ME, USA), which was placed within the BLA. For the recording of EPSC/IPSC amplitude ratio in BLA pyramidal neurons, evoked EPSC amplitude was set at − 150 to − 200 pA at − 60 mV, and evoked IPSC amplitude was set at 50–200 pA at + 15 mV. The EPSC/IPSC ratio was calculated as the maximum EPSC amplitude divided by the IPSC amplitude. For the recording of miniature EPSC (mEPSC), BLA pyramidal neurons were held at − 60 mV in the presence of sodium channel blocker (1 μM tetrodotoxin) and $GABA_A$ receptor antagonist (100 μM picrotoxin) in the bath solution. For the recording of miniature IPSC (mIPSC), BLA pyramidal neurons were held at + 15 mV in the presence of excitatory transmission blockers (50 μM D-AP5 and 10 μM CNQX) in the bath solution. To record the paired-pulse ratio of EPSC amplitudes, BLA pyramidal neurons were held at − 60 mV and evoked by the local electrical stimulation of the BLA in the presence of 100 μM picrotoxin included in the bath solution.

2.7. Stereotaxic surgery and optogenetics in acute brain slice

Four-week-old mice were anaesthetized by intraperitoneal injection of ketamine (100 mg/kg) and xylazine (20 mg/kg) and positioned using a stereotaxic instrument (Narishige, Tokyo, Japan). Eyes were protected against drying by applying ointment (Tarivid ophthalmic ointment, Santen, Osaka, Japan). A small segment of the skull above the medial prefrontal cortex (mPFC) (1.98 mm anterior to bregma and 0.2 mm lateral to the midline) was removed. Virus solutions (AAV5-CaMKIIa-ChR2-EYFP purchased from the University of North Carolina Vector Core) were pressure-injected into the mPFC (−1.2 mm from the dura, volume: 300 nl, infusion rate: 100 nl/ min) using a 10 μL Hamilton syringe driven by an infusion pump (UMP-3, World precision instruments, FL, USA). After injection, the needle was left in place for 10 min and then slowly retracted. The exposed cortex was covered with a gelatine sponge (Spongel, Astellas Pharma Inc., Tokyo, Japan), and the scalp was sutured closed.

For optogenetic examination of mPFC-BLA synaptic response, 4 weeks after viral injection, brain slices containing amygdala (300 μm) were prepared at a 35° tilt from horizontal from injected mice as described previously (Kuniishi et al., 2020). Patch-clamp recordings were taken from pyramidal-shaped principal neurons surrounded by ChR2-EYFP positive fibers in the BLA. To activate ChR2, blue light (465 nm) was delivered to the recorded cell through a 63x objective lens (duration = 0.1–3 ms, 1.8–70.7 ×10–7 J under the objective lens), using an LED lamp and its driver (LEX-2B, BrainVision, Tokyo, Japan). To record the paired-pulse ratio, picrotoxin (100 μM) was included in the ACSF. The amplitude of EPSC was measured at − 60 mV after exposure to blue light.

2.8. Immunohistochemistry

Frozen samples were sectioned at 20 μm, and the detail is described in Supplementary Information. Sections were treated with 0.1 % Triton X-100 in PBS (10 min). After incubation with 1 % H_2O_2 in PBS (60 min), sections were incubated with PBS solution containing 10 % goat serum for 60 min. Sections were then incubated with rabbit anti-VGLUT1 (1:1000, ab227805, Abcam) in PBS solution containing 10 % goat serum overnight at 4 °C, washed with PBS, and incubated with secondary antibody Alexa Fluor 568 goat anti-rabbit IgG (H+L; 1:500, Invitrogen). The density of VGLUT1-positive synaptic puncta was quantified using a BZ-H4XI image cytometry software (KEYENCE). Stained sections were analyzed using a confocal laser-scanning microscope (SPF5, Leica).

2.9. Electron microscopy

Eight-week-old male mice were deeply anesthetized with somnopentyl and transcardially perfused with 2 % glutaraldehyde and 2 % paraformaldehyde in 0.1 M cacodylate buffer (pH 7.4). Brains were removed and future fixed overnight. Coronal sections with 100 μm thick were prepared by vibratome (VT1000S; Leica). The basolateral amygdala was dissected from the coronal sections. The tissues were treated with 1 % osmium tetroxide in 0.1 M cacodylate buffer (pH 7.4) for 1 h and then stained with 3 % uranyl acetate for 1 h. Samples were dehydrated and embedded in Epon812 (TAAB). After polymerization of the resin, each tissue sample was cut into 70 nm ultrathin sections by an ultramicrotome (Leica EM UC6; Leica). Ultrathin sections were observed under an electron microscope (Tecnai Spirit; Thermo Fisher Scientific-FEI) at 120 V. The measurements of synaptic vesicle number and presynaptic PSD area were performed using ImageJ (NIH, Bethesda, Maryland). The number of synaptic vesicles was normalized by the presynaptic area.

2.10. Dystrophin isoforms restoration experiments

For intracerebroventricular microinjection of sense or antisense (ASO) morpholino oligonucleotides (Sense: 5'-GAAACCAAGGTTAGTGTCAAGCATA-3', ASO: 5'-TATGCTTGACACTAACCTTGGTTTC-3'), 30 mg/kg/single dose was administered to each mouse twice weekly for 4 weeks with a guide cannula (Eicom, Kyoto, Japan). Guide cannulas of plastic products were implanted into the lateral ventricle (0.1 mm posterior to bregma and 1.0 mm lateral to the midline, −1.5 mm from the dura, unilaterally) in 3-week-old male *mdx52* or WT mice. After

surgery, these mice were housed together. ASO dissolved in saline was administered to *mdx52* mice. *Mdx52* mice treated with sense oligonucleotides and WT mice treated with saline were used as control. Behavioural tests were performed at 8 weeks of age, and then mouse tissues were harvested within 3 days from the end of each experiment.

The amygdala, cerebral cortex, hippocampus, and cerebellum were harvested using a vibratome (VT1200, Leica), and total RNA was extracted using the RNeasy kit (Qiagen, Hilden, Germany). Aliquots of 200 ng of total RNA were used as a template for RT-PCR with complementary DNA reverse transcription kits (Applied Biosystems, Warrington, UK). For one RT-PCR reaction, 1 μL of cDNA template was mixed with 14.3 μL of water, 0.5 μL of 10 μM forward primer, 0.5 μL of 10 μM reverse primer, 1.6 μL of 2.5 mM dNTPs, 2 μL of 10 ×Ex Taq Buffer, and 0.1 μL Ex Taq HS from the Ex Taq Hot Start Version kit (Takara Bio, Shiga, Japan), using the external primers flanking the Dp427 and Dp140 sequence encoded from exon 49 forward (5'-AAACCAAGCACTCAGCCAGT-3') to exon 54 reverse (5'-CAGCAGAATAGTCCCGAAGAA-3'). For the Dp427 and Dp140 sequence, the cycling conditions were 95 °C for 3 min, 35 cycles of 94 °C for 1 min, 58 °C for 1 min, 72 °C for 1 min, and finally 72 °C for 7 min. PCR products were analyzed on 2 % agarose gels or on MultiNA, a microchip electrophoresis system (Shimadzu, Kyoto, Japan). Skipping efficiency was calculated as (exon 53-skipped transcript molarity)/(native+exon 53-skipped transcript molarity) × 100 % using MultiNA. The resulting PCR bands were extracted using a gel extraction kit (Qiagen), and direct sequencing of the PCR products was performed by the Eurofins (Tokyo, Japan).

2.11. Subcellular fractionation and Western blot

Male wild-type, *mdx23*, *mdx52* and Sense, ASO-, or mRNA-treated *mdx52* mice at 8 weeks of age were anesthetized with isoflurane, and brains were isolated. Basolateral amygdala was taken from these brains using a vibratome (VT1200, Leica), homogenized, and centrifuged to synaptosomal fractions (P2) with isolation buffer containing 320 mM sucrose, 4 mM HEPES-NaOH buffer (pH 7.3) for 30 min at 12,500 x *g* (De Camilli et al., 1983; Dunah and Standaert, 2001). P2 fractions were then resuspended with buffered sucrose, added by 9 volumes of H_2O, homogenized, and adjusted to 7.5 mM HEPES-NaOH (pH 7.4) on ice for 30 min. It was then centrifuged to synaptosomal membrane fractions (LP1) and a lysate supernatant (LS1) for 20 min at 25,000 x *g*. LS1 was centrifuged to obtain synaptic vesicle-enriched fractions (LP2) for 2 hrs at 165,000 x *g*, and LP2 was resuspended with 40 mM sucrose. LP1 was mixed with the same volume of 2 % Triton X-100, 50 μM $CaCl_2$ and 40 mM Tris-HCl (pH 7.4) and was collected by centrifugation and resuspended with 1 % Triton X-100, 50 μM $CaCl_2$ and 20 mM Tris-HCl (pH 7.4). The Pellets were collected by centrifugation and subjected to Western blotting as postsynaptic density (PSD) fractions. All procedures were performed at 4 °C.

The P2 fraction was used for Dp71, the PSD fraction was used for AMPA, NMDA and Dp427, and the LP2 fraction was used for VGLUT1 and Dp140. These fractions were determined by employing a BCA protein assay kit (Thermo Fisher Scientific). After mixing with NuPAGE LDS Sample Buffer (Thermo Fisher Scientific), cell lysates were denatured at 70 °C for 10 min, electrophoresed utilizing a NuPAGE Novex Tris-acetate gel 3–8% (Invitrogen) at 150 V for 70 min or Tris-glycine gel 4–20 % (Bio-Rad) at 150 V for 45 min, and then transferred to PVDF membranes. Following three times washes in PBS-T, the membranes were incubated with ECL western blot substrate (GE Healthcare Life Sciences). The membranes were incubated with primary antibodies, followed by incubation with a secondary antibody.

Antibodies used in Western blotting were the following: anti-dystrophin (1:50, MAB1692, Chemicon for Dp427 or 1:2000, P34a from NCNP (Mizuno et al., 1993) for Dp140 or 1:100, MANDRA1 from Wolfson Centre for Inherited Neuromuscular Disease in UK or 1:500, ab15277, Abcam for Dp71), anti-AMPA1 (1:1000, ab31232, Abcam), anti-AMPA2 (1:2000, ab206293, Abcam), anti-AMPA3 (1:1000, ab232887, Abcam), anti-NMDA1 (1:1000, D65B7, Cell Signaling), anti-NMDA2A (1:200, ab174636, Abcam), anti-NMDA2B (1:1000, ab93610, Abcam), anti-PSD-95 (1:500, GTX133091, Gene Tex), anti-VGLUT1 (1:1000, ab227805, Abcam), anti-beta-actin (A5316, 1:2000, Sigma-Aldrich) and anti-GAPDH (1:100, MAB374, Sigma-Aldrich) antibodies overnight at 4 °C. Secondary antibodies (1:5000) of anti-mouse or anti-rabbit IgG horseradish peroxidase (HRP) linked $F(ab')_2$ fragment (Cytiva) for 60 min at room temperature. The data were analyzed with Image Lab 6.0 (Bio-Rad). We quantified dystrophin protein by chemiluminescent western blotting using a standard curve. We repeated an experiment three times, and the average value was calculated.

2.12. Preparation of mRNA

Direct sequencing of the Dp140 was performed by the Eurofins (Tokyo, Japan) (Supplementary Table 1). *Dp140* and *Luc* (Negative control) mRNA-based drug was prepared through in vitro transcription (IVT) as described previously (Uchida et al., 2013). DNA templates for IVT were constructed by inserting a codon-optimized *Dp140*-expressing fragment (GenScript Japan, Tokyo, Japan), or the coding region of pGL4.13 vector (Promega Corporation, Madison, WI, USA), respectively into the pSP73 vector (Promega Corporation, Madison, WI, USA) that included a T7 promoter. Prior to the insertion, a 120-bp poly A/T sequence was cloned into the pSP73 vector downstream of the protein-coding sequence, so that mRNA possessing a 120 adenine poly (A) tail at the 3' terminal end could be obtained by a simple procedure of IVT from the pSP73-poly(A) vector. IVT was performed using mMESSAGE mMACINE T7 ULTRA Transcription Kit (Thermo Fisher Scientific, Wilmington, DE, USA). IVT prepared mRNA was purified using the spin column-based RNeasy Mini Kit (Qiagen, Hildon, Germany). RNA was quantified by absorbance spectrophotometry using a Nanodrop 2000 (Thermo Fisher Scientific, Wilmington, DE, USA). RNA quality was assessed using the Agilent 2100 Bioanalyzer chip-based capillary electrophoresis system (Agilent Technologies, Santa Clara, CA, USA).

Cos-7 cells were transfected with 36 μg of mRNA using Lipofectamine MessengerMAX (Thermo Fisher Scientific, Wilmington, DE, USA) and Opti-MEM medium (Thermo Fisher Scientific, Wilmington, DE, USA) in 10 cm dish and allowed to express for 48 h. Cos-7 cells were treated with *Luc* mRNA as a control (Fukushima et al., 2021). Treated cells were harvested with RIPA Buffer (Thermo Fisher Scientific, Wilmington, DE, USA).

2.13. mRNA-loaded polyplex nanomicelles injected into the BLA

The PEG-PAsp(DET) block copolymer was synthesized according to a previous report (Kanayama et al., 2006), and Polyplex nanomicelles were prepared as described previously (Fukushima et al., 2021). The molecular weight of PEG was 43,000 g/mol, and the polymerization degree of the PAsp(DET) portion was determined to be 63 by ^{1}H NMR analyses. Briefly, PEG-PAsp(DET) block copolymer and mRNA were dissolved in 10 mM Hepes buffer separately. The concentration of mRNA was adjusted to 300 μg/ml, and that of PEG-PAsp(DET) was adjusted in a way to obtain the ratio of 3 of the total amines in the polymers to total phosphates in mRNA (N/P ratio). The solutions of mRNA and PEG-PAsp (DET) block copolymer were mixed in a ratio of 2:1 to form the polyplex nanomicelle solution. The final mRNA concentration was 200 μg/ml.

Polyplex nanomicelle *Dp140* and *Luc* mRNA-based drugs complexes were pressure-injected into the BLA (1.4 mm anterior to bregma, 3.0 mm lateral to the midline, and −3.65 mm from the dura, volume: 2 μL) of 3-week-old male *mdx52* mice using a 10 μL Hamilton syringe driven by an infusion pump (UMP-3, World precision instruments, FL, USA). After injection, the needle was left in place for 10 min and then slowly retracted.

2.14. Statistical analysis

GraphPad Prism 8 (GraphPad Sofware, Inc., La Jolla, CA) was used to perform data analysis using unpaired two-tailed Student *t*-test, two-tailed Mann–Whitney test, one-way or two-way ANOVA analysis followed by post hoc test indicated in figure legends.

3. Results

3.1. Mdx52 mice exhibit abnormal social interaction

To clarify the hypothesis that lack of Dp140 impacts the neurobehavioural comorbidities of mice, we thus evaluated social interaction (Makinodan et al., 2012; Yizhar et al., 2011) in 8-week-old *mdx52* mice and vocal communication in *mdx52* pups on a postnatal day 7. Compared to wild-type (WT) and *mdx23* mice, *mdx52* mice exhibited a longer interaction time with a stranger mouse (Fig. 1A). To evaluate genetic and neural mechanisms underpinning social communication (Berg et al., 2018; Miranda et al., 2015), we examined ultrasonic vocalizations in pups to assess mother-pup interactions. Consistent with social interaction test results in adult *mdx52* mice, *mdx52* pups displayed more frequent and longer isolation calls during mother-pup separation when compared to WT and *mdx23* pups (Fig. 1B). No significant differences were observed between WT and *mdx23* pups (Fig. 1B), suggesting no difference in their social behaviours. These results indicated that *mdx52* mice displayed abnormal social behaviours, characteristic of ASD model mice, in adult- and infant-hood due to the lack of Dp140.

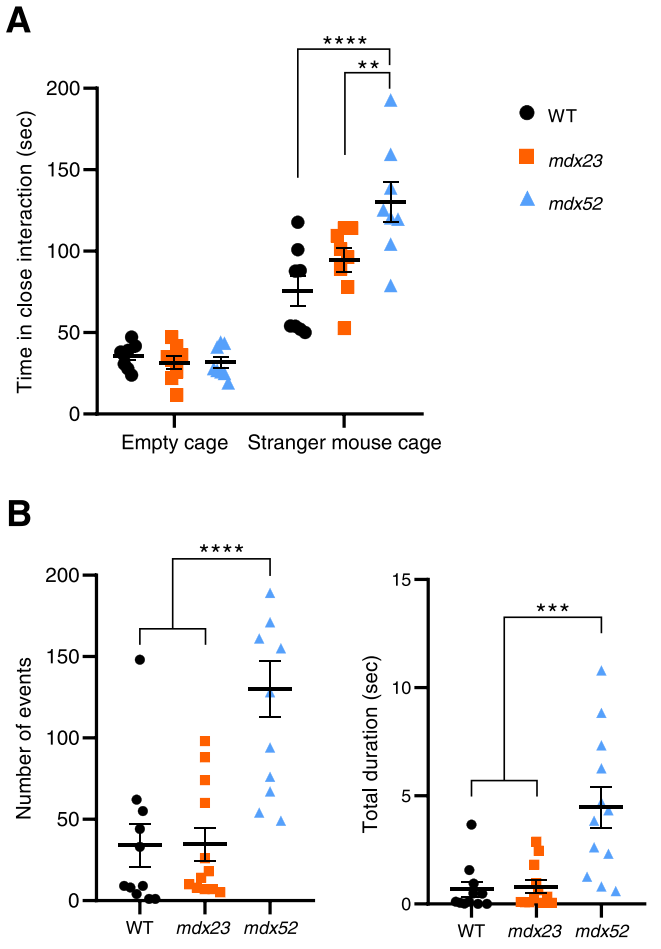

Fig. 1. Lack of Dp140 displays different behaviour between *mdx23* and *mdx52* mice in adult- and infant-hood. A. Increased social interaction in male *mdx52* mice at 8 weeks of age compared with male wild-type (WT) and *mdx23* mice at the same age; $n = 8$ mice per group; two-way ANOVA, with Dunnett. B. Increased vocal communication in male *mdx52* pups aged postnatal 7 days in the 3-min session; $n = 11$–12 pups per group; one-way ANOVA, with Dunnett. All data are presented as mean ± SEM. * * $p < 0.005$, * ** $p < 0.001$, * *** * $p < 0.0001$.

Previous studies have reported that restraint- and electrical foot-shock-induced freezing (Sekiguchi et al., 2009; Yamamoto et al., 2010) and anxiety-like behaviour in a novel environment (Vaillend and Chaussenot, 2017) are enhanced in *mdx23* mice. We, therefore, speculated that the lack of Dp140 would also be associated with and could enhance these pathological behaviours. Compared to WT mice, *mdx23* and *mdx52* mice displayed more remarkable freezing behaviour and restricted movements within the edge area in the open field test (Supplementary Fig. 2A-C). However, no significant differences were observed between *mdx23* and *mdx52* mice (Supplementary Fig. 2A-C). Average walking speed and total distance travelled were lower for *mdx23* and *mdx52* mice than WT mice, with no significant differences between the two dystrophic models (Supplementary Fig. 2D-E). In addition, we examined self-grooming behaviour, characteristic of ASD model mice (Peça et al., 2011). No significant differences were observed between *mdx23* and *mdx52* mice (Supplementary Fig. 2F). At least for the tests used in our study, these results indicated that fear/anxiety-like behaviours are similar between these two DMD mouse models, suggesting they are caused mainly by the lack of Dp427.

3.2. Excitatory-inhibitory (E-I) balance in BLA pyramidal neurons is decreased in mdx52 mice

Previous studies have reported Dp427 and Dp140 expression from each promoter of the DMD in the human BLA (Doorenweerd et al., 2017), while the dystrophin expression in brain was much lower than that in muscle (Chelly et al., 1988). Further, abnormal neurotransmission in the BLA is implicated in social behaviour and ASD pathophysiology (Amaral et al., 2008a, 2008b; Felix-Ortiz et al., 2016), and E-I imbalance in the BLA is associated with social behaviour in ASD model mice (Olmos-Serrano et al., 2010; Rubenstein and Merzenich, 2003). We hypothesized that synaptic dysfunction underpinned abnormal social communication in *mdx52* mice. To examine synaptic transmission in the BLA, we performed whole-cell patch-clamp recordings of BLA pyramidal neurons in acute brain slices from 8-week-old mice. We examined the excitatory postsynaptic current (EPSC) to inhibitory postsynaptic current (IPSC) ratio (EPSC/IPSC ratio) evoked by local electrical stimulation of the BLA. The EPSC/IPSC ratio was significantly reduced in BLA pyramidal neurons of *mdx52* mice compared to WT and mdx23 mice ($p = 0.001$), whereas no significant differences were observed between WT and *mdx23* mice (Fig. 2A).

To further characterize the alterations in glutamatergic and GABAergic transmission in *mdx52* mice, we measured miniature EPSCs (mEPSCs) and IPSCs (mIPSCs) in BLA pyramidal neurons from the slices. The frequency of mEPSCs was significantly reduced in *mdx52* mice compared to that in WT and *mdx23* mice (Fig. 2B-C, $p = 0.0228$). The frequency of mIPSCs was significantly reduced in both *mdx23* and *mdx52* mice compared to that in WT mice, whereas no significant differences were observed in the mIPSC frequency and amplitude between *mdx23* and *mdx52* mice (Fig. 2D). To examine excitatory presynaptic function in *mdx52* mice, we assessed the paired-pulse ratio in BLA pyramidal neurons evoked by local electrical stimulation. The paired-pulse ratio of EPSCs at a 50 ms interval was significantly lower in *mdx52* mice than in WT and *mdx23* mice (Fig. 2E), suggesting that the presynaptic plasticity in the BLA excitatory synapses is changed in *mdx52* mice, possibly due to the lack of Dp140.

3.3. Presynaptic plasticity of the medial prefrontal cortex (mPFC)-BLA projections is disrupted in mdx52 mice

The lack of Dp140 has been reported to underpin abnormal nervous

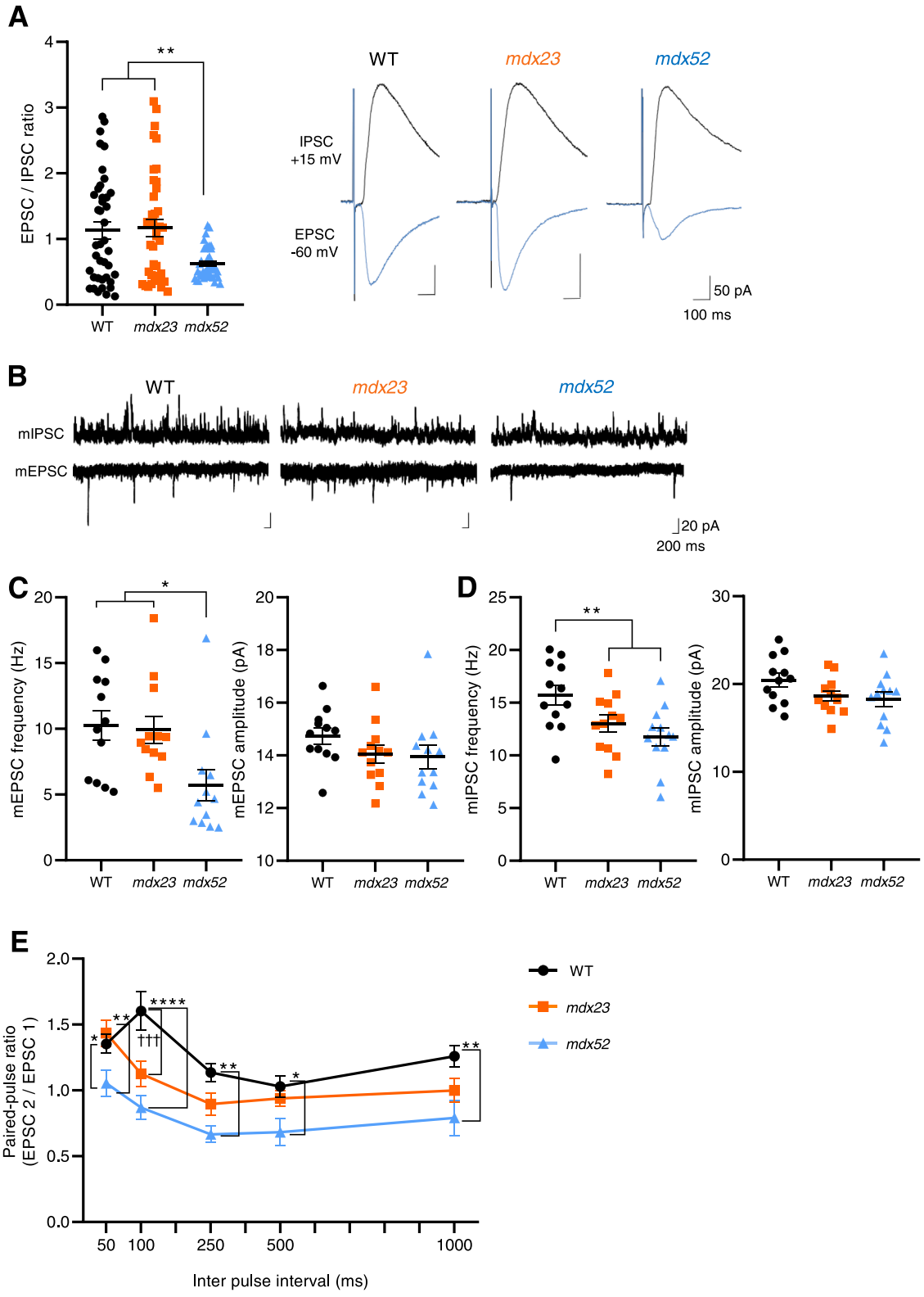

Fig. 2. Lack of Dp140 impairs excitatory-inhibitory (E-I) balance and glutamatergic transmission in the BLA pyramidal neurons. A. Excitatory postsynaptic current/inhibitory postsynaptic current (EPSC/IPSC) amplitude ratio is significantly lower in BLA pyramidal neurons of male *mdx52* mice at 8 weeks of age than in those of wild-type and *mdx23* mice at the same age; $n = 40$ neurons from four mice per group; one-way ANOVA, with Dunnett. B. mIPSC and mEPSC traces from male wild-type, *mdx23* and *mdx52* mice at 8 weeks of age, during whole-cell patch-clamp recording at + 15 mV and − 60 mV. C. Reduced mEPSC frequency but not amplitude in BLA pyramidal neurons of male *mdx52* compared with *mdx23* mice at 8 weeks of age; $n = 12$ neurons from four mice per group; one-way ANOVA, with Dunnett. D. Frequency and amplitude of mIPSC were not different between male *mdx23* and *mdx52* mice at 8 weeks of age; $n = 12$ neurons from four mice per group; one-way ANOVA, with Dunnett. **E.** Paired-pulse ratio is significantly lower in male *mdx52* mice at 8 weeks of age than in male wild-type and *mdx23* mice at the same age; $n = 12$ neurons from four mice per group; two-way ANOVA, with Dunnett. All data are presented as mean ± SEM. * $p < 0.05$, * * $p < 0.005$, * ** * $p < 0.0001$, $^{\dagger\dagger\dagger}p < 0.001$.

system tract morphology in human DMD patients (Doorenweerd et al., 2014). We, therefore, hypothesized that abnormal excitatory neural networks underscored abnormal social communication in *mdx52* mice. To evaluate pathway-specific glutamatergic responses in social brain circuits, we isolated excitatory synaptic transmission in the mPFC-BLA pathway, which has been implicated in social deficits in ASD model mice (Felix-Ortiz et al., 2016; Huang et al., 2016), using patch-clamp and optogenetic methods. Serotype 5 adeno-associated virus (AAV) expressing channelrhodopsin-2 (ChR2) fused to an enhanced yellow fluorescent protein (eYFP) was injected into the mPFC under the control of CaMKIIa promotor for targeting glutamatergic projection neurons. Afferent axon terminals from the mPFC were observed in the BLA 4 weeks post-AAV injection (Fig. 3A and Supplementary Fig. 3A). We performed whole-cell patch-clamp recordings and examined blue light-evoked EPSCs reflecting excitatory presynaptic responses in BLA pyramidal neurons in these mice (Fig. 3B). The Paired-pulse ratios in

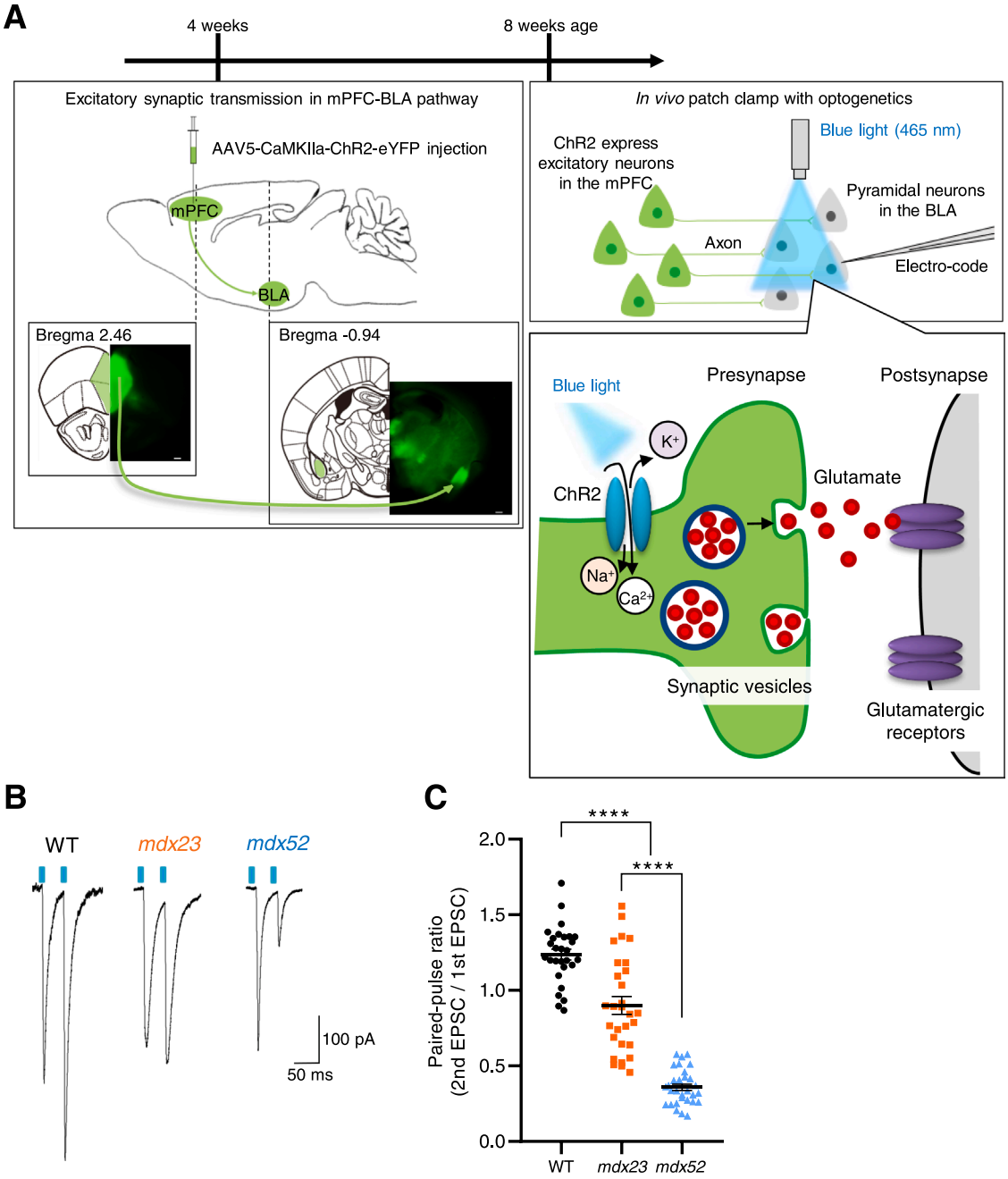

Fig. 3. Lack of Dp140 impairs glutamate emission depleted at the presynaptic terminals projecting from the medial prefrontal cortex (mPFC). A. Optogenetic analysis of mPFC inputs to the BLA in male wild-type, *mdx23* and *mdx52* mice at 8 weeks of age. Experimental design for optogenetic activation of mPFC-BLA projections. Scale bar, 500 μm. To target glutamatergic projection neurons, the mPFC was transduced with Channelrhodopsin (ChR)2-eYFP under the control of the CaMKIIα promoter. ChR2, delivered by AAV5 vector injections in the mPFC, functions as a blue light-gated ion channel in the axon terminal. Glutamate is released from the axon terminals, and glutamatergic transmission is observed in the BLA pyramidal neuron under blue light irradiation. B. Paired-pulse ratio with optogenetics confirms a reduction of glutamate emission in male *mdx52* BLA pyramidal neurons projected from the mPFC in response to blue light irradiation from a 63-objective lens (blue square), during whole-cell patch-clamp recording at − 60 mV. C. Paired-pulse ratio at 50-ms interval is significantly lower in male *mdx52* mice at 8 weeks of age than in male wild-type and *mdx23* mice at the same age in the mPFC-BLA pathway; $n = 28–30$ neurons from three mice per group; one-way ANOVA, with Dunnett. All data are presented as mean ± SEM. * ** * $p < 0.0001$.

mPFC-BLA projection in *mdx52* mice were significantly lower than in WT and *mdx23* mice (Fig. 3C), and those in *mdx23* mice were also lower than those in WT mice (Fig. 3C). However, these differences were observed at only 50 ms pulse interval (Supplementary Fig. 3B). These results indicated that short-term presynaptic plasticity (Zucker and Regehr, 2002), which might be influenced by the factors such as the number of immediately releasable vesicles and the vesicle release probability of mPFC-BLA projections, is possibly disrupted due to the lack of Dp427 and is exacerbated by the additional lack of Dp140 in *mdx52* mice.

3.4. Vesicular glutamate transporter 1 (VGLUT1) protein levels in the BLA are lower in mdx52 mice than in mdx23 mice

Reduced glutamate release has been implicated in ASD pathophysiology in murine models (Heise et al., 2016; Smith et al., 2011). The loss of VGLUT1, which accumulates glutamate into synaptic vesicles, appears to have silenced the population of glutamate release sites in BLA and substantially reduced the frequency of mEPSCs (Fremeau et al., 2004a, 2004b). We thus analyzed the expression of VGLUT1 and glutamate receptor subunits including AMPA and NMDA, using biochemically purified synaptic vesicle-enriched fractions (LP2) and postsynaptic density (PSD) fractions from the BLA of these mice. As shown in Fig. 4A, VGLUT1 expression in *mdx52* was lower than that in *mdx23*, and these differences were statistically significant (Fig. 4A, $p = 0.0333$). Since Dp140 expression might differ between *mdx23* and *mdx52*, we thought it was important to compare VGLUT1 expression levels between *mdx23* and *mdx52* for the evaluation of the effect of Dp140 expression on VGLUT1 levels. Additionally, VGLUT1 expression in WT was comparable to that in *mdx23*, and it was lower in *mdx52* than in WT but was non-significant (Fig. 4A).

To further confirm these results, we also measured the number of VGLUT1-labeled puncta in the BLA, and found that in *mdx52*, it was significantly less compared to WT and *mdx23* mice (Fig. 4B and C). The difference in the number of VGLUT1 puncta between WT and *mdx23* was smaller than that between WT and *mdx52*, showing a similar trend to the results in Fig. 4A. No significant differences were observed in glutamatergic receptor expression (Supplementary Fig. 4). These results suggest a difference in VGLUT1 expression between *mdx23* and *mdx52* mice and a less clear difference between WT and *mdx23*.

3.5. Synaptic vesicle number in BLA neuronal presynaptic boutons is lower in mdx52 mice than in mdx23 mice

Given that ASD model mice exhibit morphological defects and abnormal synaptic plasticity (Hansel, 2019), we examined the effects of the lack of Dp140 on neuronal morphological abnormalities underpinning altered glutamatergic neurotransmission in *mdx52* mice. To assess histology, we performed haematoxylin and eosin, and Nissl staining. No histological differences were observed in the BLA between *mdx23* and *mdx52* mice (Supplementary Fig. 5A). To investigate neuronal morphology, we quantified the number of Golgi-stained BLA pyramidal neurons ($n = 12$–13 dendrites each BLA pyramidal neuron of three mice per group). The number of protrusions in the BLA and of mature mushroom spines in dendrites was significantly decreased to a similar extent in *mdx23* and *mdx52* mice compared to that in WT mice ($p < 0.0001$), while no significant differences were noted between *mdx23* and *mdx52* mice (Supplementary Fig. 5B-C).

To analyze the number of glutamatergic synaptic vesicles including VGLUT1 at individual presynaptic terminals and excitatory synapse morphology in BLA neurons associated with a lack of Dp140, we investigated asymmetric (excitatory) synapses using electron microscopy (Fig. 4D). The number of docked vesicles less than 100 nm from the active zone, the region in the presynaptic bouton that mediates neurotransmitter release, and the number of vesicles in the reserve pools more than 100 nm away from the active zone were significantly lower in BLA neurons of *mdx23* and *mdx52* mice than WT mice (Fig. 4E, $p < 0.0001$). However, no significant difference was observed in the number of docked vesicles in BLA neurons between *mdx23* and *mdx52* mice (data not shown). This reduction in the number of reserve vesicles is likely to have contributed to the observed altered optogenetic paired-pulse ratio of EPSCs at a 50 ms interval in *mdx52* mice (Fig. 3C). Further, no significant differences were observed in the mean values of the presynaptic area, PSD length, and PSD width between WT, *mdx23,* and *mdx52* mice (Supplementary Fig. 6A-B). These results suggest that the reserve pools of presynaptic vesicles including VGLUT1 in the BLA are reduced due to the lack of Dp140 in the *mdx52* mice.

3.6. Induction of exon 53 skipping and partial restoration of Dp140 isoform expression ameliorate deficits in glutamatergic transmission and social behaviour in mdx52 mice

To elucidate the effects of rescuing internally deleted Dp140 on social behaviour, EPSC/IPSC ratio and paired-pulse ratio, antisense phosphorodiamidate morpholino oligonucleotide (ASO) was injected intracerebroventricularly to induce exon 53 skipping and promote partial recovery of both Dp427 and Dp140 expression (Alter et al., 2006a, 2006b). Exon skipping treatment is a therapeutic approach using splice-switching oligonucleotides to effectively target the *DMD* gene and restore the reading frame of the *DMD* transcript. Restoration of internally deleted Dp427 following exon skipping using ASO is reported to ameliorate physiological function in brain (Sekiguchi et al., 2009) and muscles (Aoki et al., 2010a, 2010b), by producing shortened dystrophin molecules similar to those produced in the milder Becker muscular dystrophy allelic variant of DMD. However, it remains unclear whether the partial restoration of internally deleted Dp140 following exon 53 skipping using ASO ameliorates glutamatergic neurotransmission or improves social behaviour in *mdx52* mice. ASO dissolved in saline was administered intracerebroventricularly with a guide cannula in 3-week--old *mdx52* mice twice a week for 4 weeks. *Mdx52* mice treated with sense oligonucleotides (Sense) and WT mice treated with saline were used as control. WT mice were also using the same cannula as the Sense- and ASO-treated *mdx52* mice. The brain was harvested 1 week after the final infusion (Fig. 5A).

To confirm Dp140 expression, we performed RT-PCR and western blotting analysis of the BLA of ASO-treated *mdx52* mice. As expected, ASO-treated bands were a lower molecular weight than those of native *Dp427* and *Dp140* mRNA in the BLA, indicating effective exon skipping was induced (Fig. 5B). We observed that ASO targeted the cryptic splice site of the 5′part of exon 53, indicating the absence of 78 bp in one transcript. Direct sequencing of the PCR product revealed the junction of exons 53 and 54, and the production of an in-frame *DMD* transcript, expected to result in partial restoration of internally deleted Dp140 (Fig. 5B). We also assessed exon 53 skipping efficiency by RT-PCR using ASO-treated *mdx52* mice of BLA, cerebral cortex, hippocampus and cerebellum (Fig. 5B and Supplementary Fig. 7A). The level of the exon 53 skipping efficiency was 8.71 ± 1.73 % in the BLA, 10.15 ± 2.81 % in the cerebral cortex, 8.89 ± 2.52 % in the hippocampus and 10.51 ± 0.86% in the cerebellum of ASO-treated *mdx52* mice (Fig. 5C and Supplementary Fig. 7B, mean ± SD). Additionally, we have conducted the western blot, and could observe 1.07 % levels of internally deleted Dp427 and 4.6 % levels of internally deleted Dp140 protein expression in the BLA of ASO-treated *mdx52* mice compared with the normal control after calculation using the standard curve (Fig. 5D and Supplementary Fig. 8), suggesting that the expressions of dystrophin protein were consistent with RNA levels, and that ASO administration partially restored internally deleted Dp140 protein as well as internally deleted Dp427 protein. We could not perform protein expression analysis using all ASO-treated samples since the measurement of EPSC/IPSC ratio and paired-pulse ratio were required whole brain tissue to avoid damaging the neural circuits. However, all three ASO-treated brains clearly showed an increase of dystrophin expression (Fig. 5D). Therefore, the

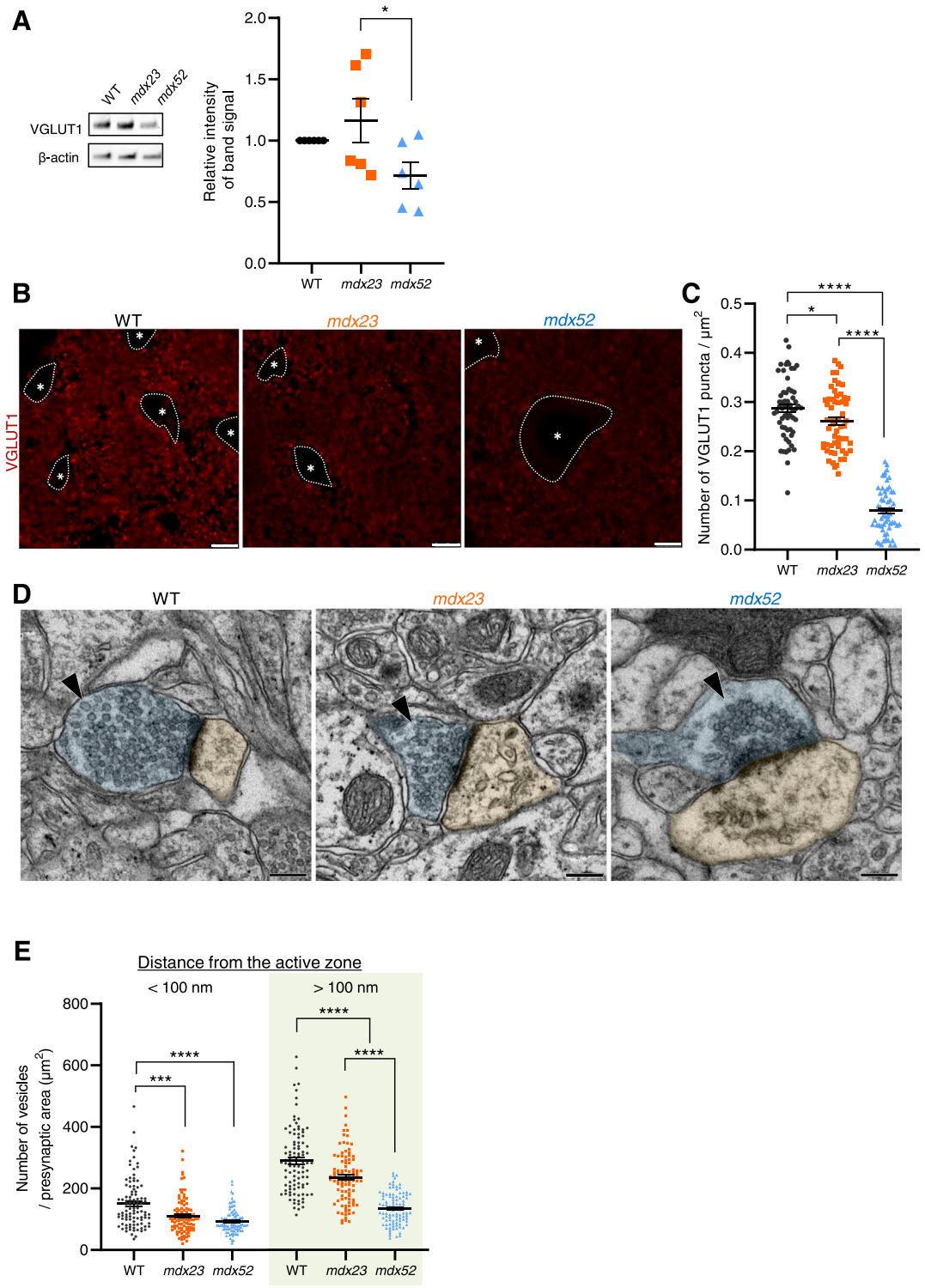

Fig. 4. Lack of Dp140 impairs vesicular glutamate transporter 1 (VGLUT1) at the presynapse and affects the number of synaptic vesicles at glutamatergic presynaptic boutons in the BLA. A. The protein levels of VGLUT1 at the presynapse in the BLA are reduced in male *mdx52* at 8 weeks of age compared to male *mdx23* mice at the same age. The LP2 fractions were subjected to western blot analysis using anti-VGLUT1 and anti-β-actin antibodies (as an internal standard); $n = 6$ samples per group; one-way ANOVA, with Dunnett. B. Representative images in the BLA sections from male wild-type, *mdx23* and *mdx52* mice at 8 weeks of age stained with VGLUT1 (red dots), for excitatory presynaptic markers. Scale bar, 5 µm. * Post-synapse soma. C. Quantification of the density of VGLUT1-positive synaptic puncta in the BLA using 60x objective equipped with a BZ-H4XI image cytometry software. $n = 60$ sections from three male mice at 8 weeks of age per group; one-way ANOVA, with Dunnett. D. Example of electron micrographs depicting the synaptic contact with presynaptic vesicles (arrowheads), presynaptic spine (blue area), and postsynaptic spine (yellow area) in the BLA of male wild-type, *mdx23* and *mdx52* mice at 8 weeks of age; scale bar, 200 nm. E. Quantification of the number of presynaptic vesicles in the BLA with an electron microscope. The number of docked vesicles (< 100 nm from the active zone) is significantly lower in male *mdx52* and *mdx23* mice at 8 weeks of age than in male wild-type mice at the same age. The number of vesicles in the reserve pools (> 100 nm from the active zone) is significantly lower in male *mdx52* mice at 8 weeks of age than in male wild-type and *mdx23* mice at the same age. $n = 100$ glutamatergic synapses each BLA spines of 3 mice per group; one-way ANOVA, with Dunnett. All data are presented as mean ± SEM. * $p < 0.05$, * ** $p < 0.001$, * ** * $p < 0.0001$.

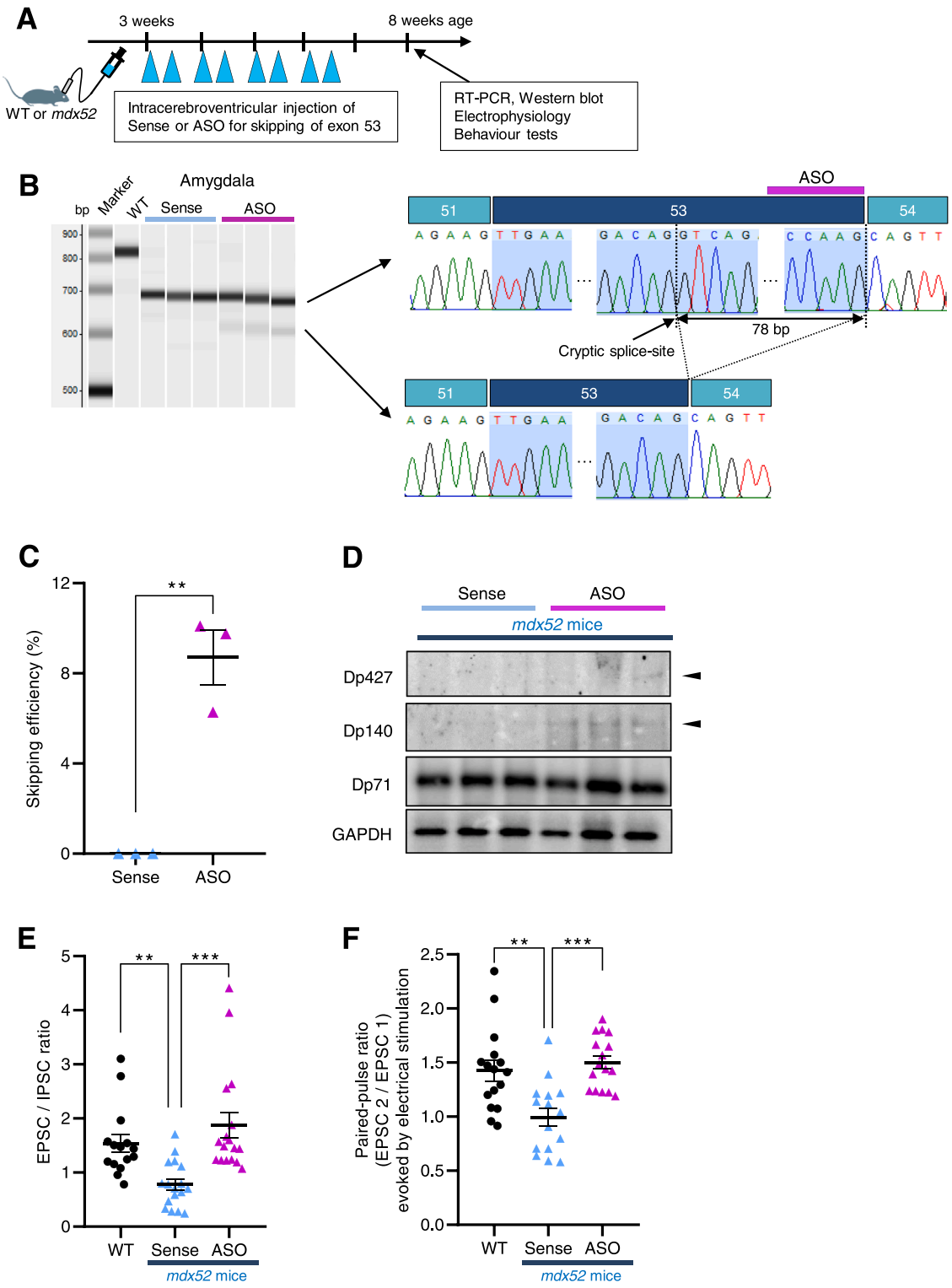

Fig. 5. Antisense morpholino oligonucleotide (ASO) induces internally deleted Dp140 expression in the brain of *mdx52* mice, and glutamate emission in the mPFC-BLA pathway is increased in ASO-treated *mdx52* mice. A. The administration of sense or antisense oligonucleotides via intracerebroventricular injection was started at 3 weeks of age and finished at 7 weeks of age. 30 mg/kg/single dose was administered with a guide cannula. B. Skipping efficiency of exon 53 is assessed by RT-PCR for Sense- or ASO-treated *mdx52* mice at 8 weeks of age of the BLA. The sequence of exon 53 skipping in ASO-treated *mdx52* mice at 8 weeks of age was confirmed. ASO targeted cryptic splice-site of the 5′ part of the exon 53, indicating the absence of 78 bp in one transcript (upper column). Sequencing of the product revealed the junction of exons 53 and 54 (lower column). C. The quantification of the exon 53 skipping levels of the BLA; n= 3 mice; two-tailed t-test. D. Western blot analysis showing the appearance of internally deleted Dp427, Dp140 and Dp71 bands of a similar size to native Dp140 in the BLA of ASO-treated *mdx52* mice at 8 weeks of age, using anti-dystrophin and anti-GAPDH antibodies (as an internal standard). E. EPSC/IPSC ratio was improved in ASO-treated *mdx52* mice at 8 weeks of age; n=15–17 neurons from five mice per group; one-way ANOVA, with Dunnett. F. Paired-pulse ratio at 50-ms intervals in the BLA pyramidal neurons evoked by the local electrical stimulation is improved in ASO-treated *mdx52* mice at 8 weeks of age; n=15–16 neurons from five mice per group; one-way ANOVA, with Dunnett. G. Optogenetic analysis of mPFC inputs to the BLA in Sense- or ASO-treated *mdx52* mice at 8 weeks of age. AAV5-CaMKIIa-ChR2-eYFP were injected into the mPFC at 3

weeks of age. The administration of Sense or ASO via intracerebroventricular injection was started at 3 weeks of age and finished at 7 weeks of age. H. Paired-pulse ratio with optogenetics confirms the glutamate emission in the mice BLA pyramidal neuron projected from mPFC in response to blue light irradiation (blue square), during whole-cell patch-clamp recording at − 60 mV. I. Paired-pulse ratio at 50-ms interval with optogenetics in mPFC-BLA pathway was improved in ASO-treated *mdx52* mice at 8 weeks of age; $n = 9$ neurons from three mice per group; one-way ANOVA, with Dunnett. J. Western blot showed the appearance of VGLUT1 bands in the BLA of the mice at 8 weeks of age. The LP2 fractions were subjected to western blot analysis using anti-VGLUT1 and anti-GAPDH antibodies (as an internal standard); n=4–6 mice per group; one-way ANOVA, with Dunnett. K. The social interaction was improved in ASO-treated *mdx52* mice at 8 weeks of age; n=10 mice per group; two-way ANOVA, with Dunnett. All data are presented as mean ± SEM. * $p < 0.05$, * * $p < 0.005$, * ** $p < 0.001$, * ** * $p < 0.0001$.

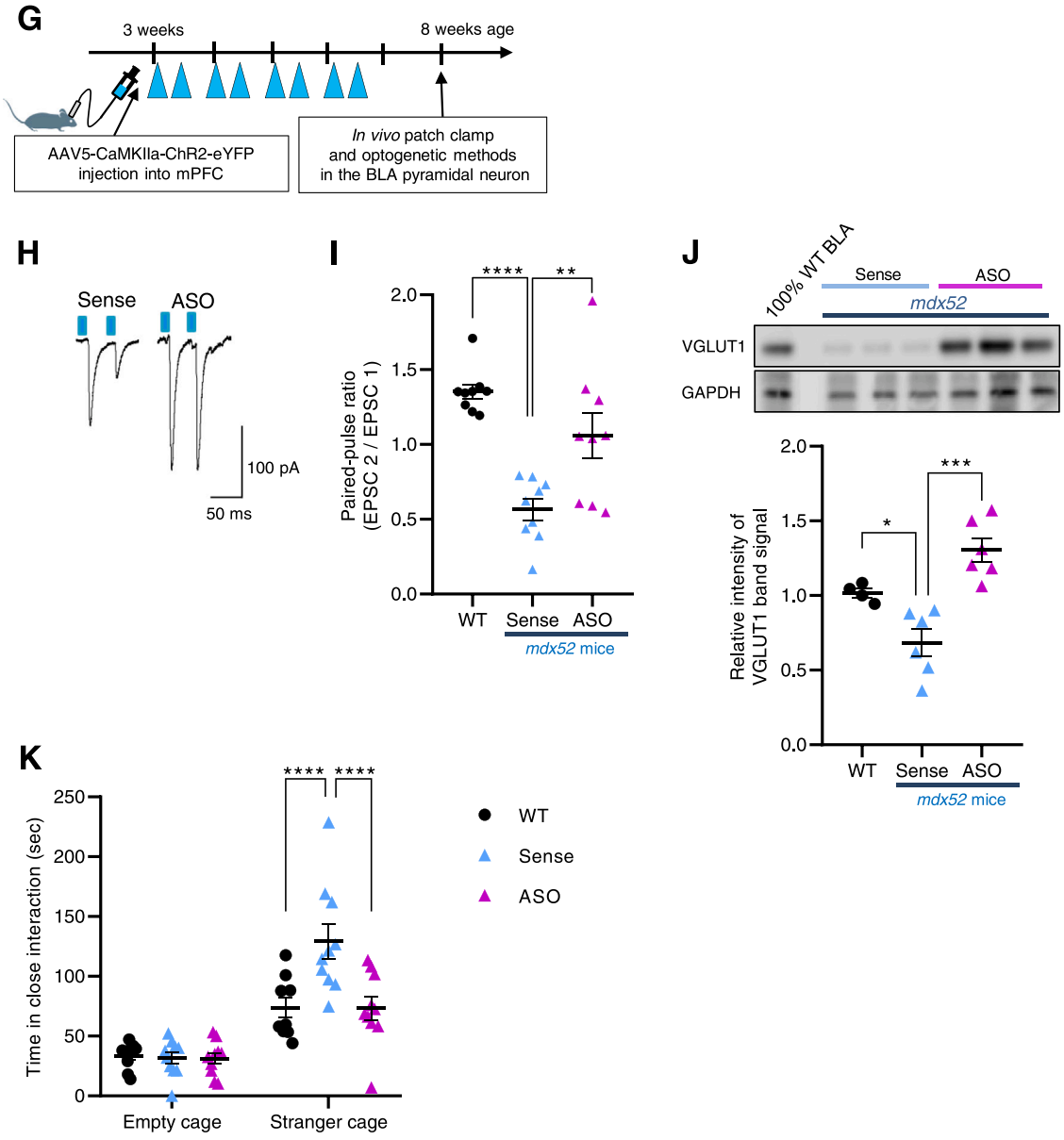

Fig. 5. (*continued*).

same tendency would be expectable in remained samples.

To evaluate the effects of ASO treatment on synaptic dysfunction in *mdx52* mice, we examined the EPSC/IPSC and paired-pulse ratios and mEPSCs. EPSC/IPSC and paired-pulse ratios were recovered in ASO-treated *mdx52* mice (Fig. 5E-F), although no significant difference was observed in mEPSC frequency between Sense- and ASO-treated *mdx52* mice (Supplementary Fig. 9A). Regarding the effects of ASO treatment on mPFC-BLA pathway-specific glutamatergic release (Fig. 5G), we found that the paired-pulse ratio in the mPFC-BLA pathway was partially recovered in ASO-treated *mdx52* mice (Fig. 5H-I). In addition, VGLUT1 protein levels in the BLA were elevated in ASO-treated *mdx52* mice (Fig. 5J), possibly indicating altered glutamatergic release following the partial restoration of Dp140 in the BLA. We also assessed the effects of ASO treatment on abnormal behaviours in *mdx52* mice with the behavioural tests that we previously demonstrated. Deficits in social behaviour were ameliorated in ASO-treated *mdx52* mice (Fig. 5K, $p < 0.0001$). No significant differences were observed in fear responses, anxiety-like behaviour, and motor function between Sense- and ASO-treated *mdx52* mice (Supplementary Fig. 9B-F).

3.7. *Dp140 overexpression in the BLA normalizes glutamatergic transmission and social behaviour in mdx52 mice*

We employed a different mRNA-based treatment to further examine whether amelioration of the glutamatergic transmission and social behaviour observed after ASO treatment was due to restoration of

internally deleted Dp140 or Dp427 or both of the dystrophin isoforms in the BLA of *mdx52* mice. Bioanalyzer analysis of full-length *Dp140* and *Luc* mRNA-based drugs indicated that both mRNAs were produced, and protein expression in mRNA-transfected cells confirmed Dp140 expression (Fig. 6A-B).

To elucidate whether the lack of Dp140 underpinned excitatory synaptic dysfunction and abnormal social behaviour in *mdx52* mice, *Dp140* mRNA was injected into the BLA using polyplex nanomicelles to promote recovery of Dp140 expression (Fig. 6C). We could confirm that the *Dp140* mRNA treatment restored 10.9 % levels of the Dp140 protein expression, but not Dp427 protein expression, after calculation using the standard curve (Fig. 6D and Supplementary Fig. 10). EPSC/IPSC, paired-pulse ratios in BLA pyramidal neurons and VGLUT1 protein levels in the BLA were elevated in *Dp140* mRNA-treated *mdx52* mice (Fig. 6E-G). We also observed normalization of social behaviour in *Dp140* mRNA-treated *mdx52* mice (Fig. 6H, $p < 0.0001$), whereas no significant differences were observed in fear response, anxiety-like behaviour, and motor function between *Luc* and *Dp140* mRNA-treated *mdx52* mice (Supplementary Fig. 11). These results suggest that restoration of Dp140 in the BLA is associated with glutamatergic transmission deficit and abnormal behaviour in 8-week-old *mdx52* mice, equivalent to adolescent and young adult in humans.

4. Discussion

We utilized two DMD mouse models to examine synaptic function in the presence or absence of brain Dp140 isoforms. Our findings suggest for the first time that the lack of Dp140 is associated with abnormal social behaviours and decreased glutamatergic transmission in *mdx52* mice, which are implicated in ASD-like symptoms in human DMD lacking brain Dp140 isoform (Bardoni et al., 2000a, 2000b; Chamova et al., 2013; Felisari et al., 2000; Ricotti et al., 2016). Furthermore, we observed that ASD-like behaviours in *mdx52* mice were improved by the partial restoration of Dp140 following both exon 53 skipping and the mRNA therapeutics-mediated Dp140 overexpression.

In human, Dp427 and Dp140 are expressed in the amygdala (Doorenweerd et al., 2017), and their deficiency is associated with emotional and social behaviours linked to ASD symptoms (Baron-Cohen et al., 2000a, 2000b). E-I imbalance in the BLA and mPFC-BLA pathway is involved in social deficits in ASD model mice (Chao et al., 2010; Huang et al., 2016; Yizhar et al., 2011). Further, mPFC-BLA projections are implicated in the processing of emotional valence and social information (Huang et al., 2020). In view of the central role of the human amygdala in several of neurobehavioural comorbidities and the dystrophin isoform expression in amygdala, we investigated the molecular functions of the murine amygdala. We previously reported that $GABA_A$ receptor subunit cluster number was reduced in the BLA of *mdx23* mice, and the lack of Dp427 impaired amygdala GABAergic transmission and enhanced defensive behaviour (Sekiguchi et al., 2009). In this study, we confirmed abnormal postsynaptic GABAergic transmission in the BLA of *mdx52* mice, consistent with reduced GABAergic transmission modulated by the lack of Dp427 (Kueh et al., 2011; Sekiguchi et al., 2009). Furthermore, we demonstrate abnormal presynaptic glutamatergic transmission modulated by the lack of Dp140 in the BLA of *mdx52* mice for the first time. Notably, we observed that the presynaptic plasticity of mPFC-BLA pathway was disrupted, and the number of synaptic vesicles at glutamatergic presynapses decreased in the BLA *mdx52* mice. The reduced reserve pools of synaptic vesicles in our study are consistent with previous results in VGLUT1 knockout mice (Fremeau et al., 2004a). As hypothesized, the reduced number of synaptic vesicles including VGLUT1 in *mdx52* mice may underlie common pathophysiology in neurodevelopmental disorders such as ASD and ADHD (John et al., 2020). We speculate that the reduced presynaptic glutamatergic transmission and postsynaptic GABAergic transmission associated with Dp140 and Dp427 may underpin abnormal neural networks in *mdx52* mice.

Our study predominantly focused on abnormal glutamatergic release in BLA presynapses in *mdx52* mice. It remains unclear how the lack of Dp140 contributes to the reduction in the reserve pools of synaptic vesicles including VGLUT1 at BLA presynapses. Immunohistochemical analyses have indicated that Dp140 is located in astrocytic processes in the neuropil, glial end-feet along blood vessels (Caudal et al., 2020; Lidov et al., 1995), neurons (Blake et al., 1998) and oligodendrocytes (Aranmolate et al., 2017a, 2017b). Dp140 is increased during astrocytic and neuronal differentiation (Romo-Yáñez et al., 2020). Dp140 in astrocytes is thought to contribute to a glutamatergic release (Patel et al., 2019), and genes co-expressed with Dp140 are enriched in GO-terms related to early neurodevelopment via regulation of neuronal projection morphogenesis (Doorenweerd et al., 2017). Dystrophin short isoforms in the brain, including Dp140 and Dp71, modulate dystrophin-associated proteins (Moukhles and Carbonetto, 2001; Waite et al., 2012), including alpha-dystrobrevin-1 (Blake et al., 1999; Greenberg et al., 1996), which directly binds to the C-terminus of dystrophin short isoforms and dysbindin-1 (Benson et al., 2001). Dysbindin-1 has been implicated in glutamate release in the brains of schizophrenia patients and model mice (Saggu et al., 2013; Talbot et al., 2006). In addition, Dp71 short isoform in astrocytes is also thought to play a role in glutamatergic release (Chaussenot et al., 2019; Miranda et al., 2011), and the Dp40 shortest isoform is also implicated in glutamatergic synaptic vesicle trafficking proteins at presynapses (Tozawa et al., 2012). We conjecture that the Dp140 in astrocytes and/or presynaptic neurons in the BLA modulates glutamatergic release by synaptic vesicles. Based on our current understanding of astrocyte-mediated presynaptic modulation of glutamatergic transmission, we propose that abnormal glutamate release is affected by the lack of Dp140 in neurons and potentially also in astrocytes. In this regard, VGLUT1-containing synaptic vesicles including glutamate represent sites for glutamatergic transmission from astrocytes to neurons (Bezzi et al., 2004). Moreover, it has been reported that astrocytes release distinct neurotransmitters such as glutamate and GABA; these glia-derived neurotransmitters may act on neurons to regulate synaptic transmission and plasticity via various mechanisms (Araque et al., 2014a, 2014b). Therefore, we speculate that the Dp140 and dystrophin-associated proteins may contribute to presynaptic inhibition, regulate glutamate recycling and release into synaptic vesicles, and modulate neuron-astrocyte interactions in the BLA.

However, our study has several limitations for evaluating the function of Dp140. First, developing specific anti-Dp140 antibodies is challenging, given that the amino acid sequence of Dp140 is identical to that of Dp427 in mice. Second, since the expressions of Dp427 and Dp140 were not clearly detected by immunohistostaining, we could not identify the localization of these proteins. In our experiments, dystrophin protein levels appeared consistent with the efficiencies of exon 53 skipping in the BLA (Fig. 5). However, since the expressions of both Dp140 and Dp427 protein were quite low (Fig. 5D), this might be insufficient to detect these proteins by immunohistostaining. The potential reasons were that the degree of dystrophin protein restoration in this study was much lower than that in previous studies (Sekiguchi et al., 2009). Therefore, we assumed that there was not sufficient dystrophin protein content to identify the correct signal by the immunohistochemical staining. We also interpreted the high background signal in the brain as a contributing factor to the failure of this immunostaining. Lastly, Dp140-specific knockout mice are currently unavailable, limiting further investigations of the molecular function of Dp140. Further work is needed to clarify how Dp140 regulates glutamatergic transmission in the BLA.

In conclusion, the lack of Dp140 resulted in decreased glutamatergic transmission in the mPFC-BLA pathway and reduced VGLUT1 expression at presynapses in the BLA of *mdx52* mice. Restoration of Dp140 rescued abnormal glutamatergic transmission and social behaviour observed in *mdx52* mice. These results suggest that the restoration of Dp140 may provide a novel therapeutic option for DMD patients with ASD-like symptoms. This comorbidity affects approximately 30 % of

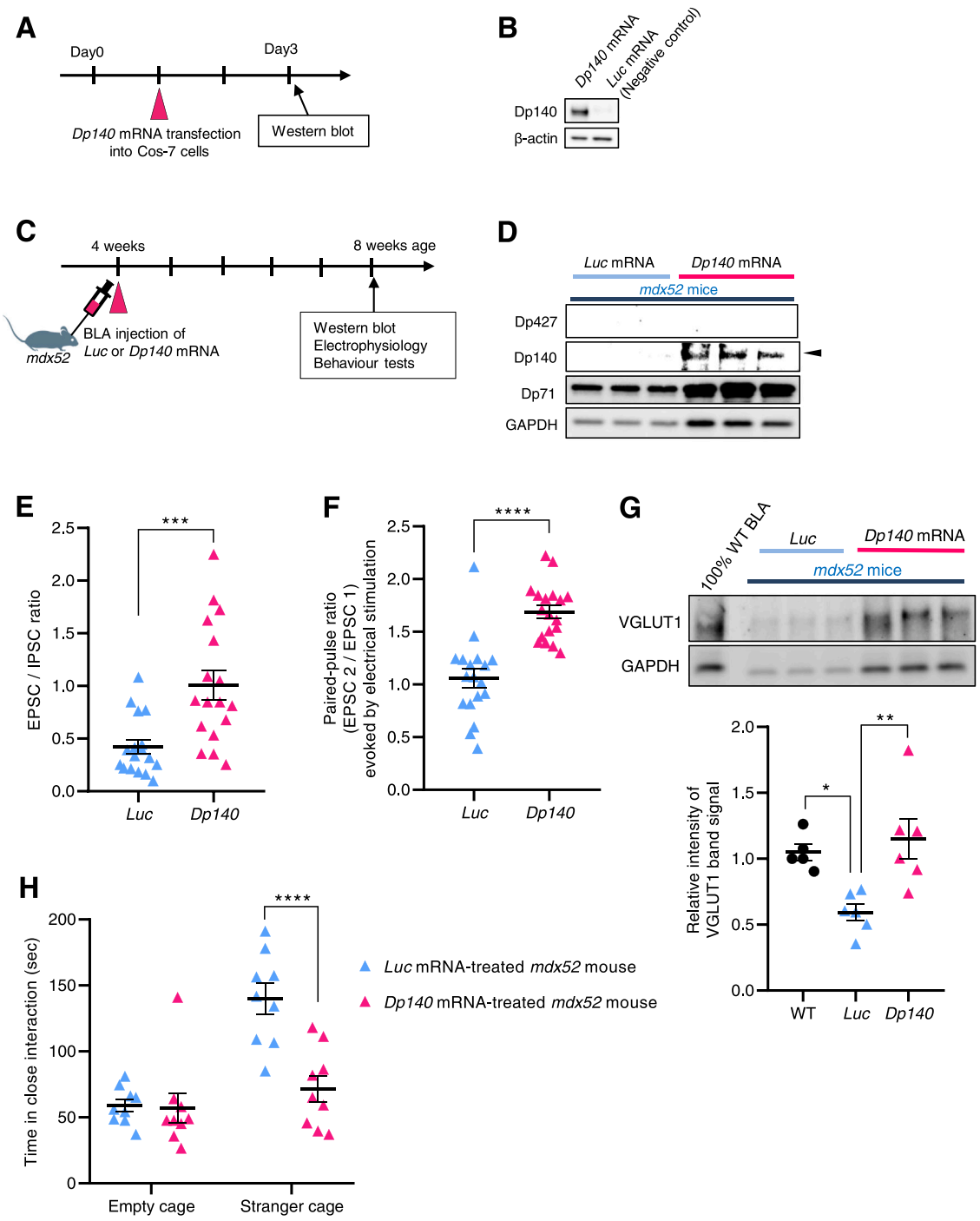

Fig. 6. *Dp140* expression in the BLA of *mdx52* mice rescues glutamatergic transmission and abnormal social interaction. A. Experimental model of *Dp140* mRNA introduction into COS-7 cells; The cells were transfected with *Dp140* mRNA or *Luc* mRNA (as a negative control)-based drugs on day 1 and harvested and processed for western blot analysis on day 3. B. Western blot analysis of Dp140 bands in the *Dp140* mRNA-transfected COS-7 cells using anti-dystrophin (P34a) and anti-β-actin antibodies (as an internal standard). C. Experimental model of *Luc* or *Dp140* mRNA-based drug administration into the male *mdx52* BLA at 4 weeks of age. D. Western blot analysis shows the appearance of Dp427, Dp140 and Dp71 bands in BLA of *Dp140* mRNA-treated *mdx52* mice at 8 weeks of age, using anti-dystrophin and anti-GAPDH antibodies (as an internal standard). E. EPSC/IPSC ratio is improved in *Dp140* mRNA-treated *mdx52* mice at 8 weeks of age; $n = 17$ neurons from six mice per group; two-tailed *t*-test. F. Paired-pulse ratio at 50-ms intervals in the BLA pyramidal neurons evoked by the local electrical stimulation is improved in ASO-treated *mdx52* mice at 8 weeks of age; $n = 18$ neurons from six mice per group; two-tailed *t*-test. G. Western blot showing the appearance of VGLUT1 bands in the BLA of the mice at 8 weeks of age; $n = 5$–6 mice per group; one-way ANOVA, with Dunnett. H. The social interaction is normalized in *Dp140* mRNA-treated *mdx52* mice at 8 weeks of age; $n = 9$ mice per group; two-way ANOVA, with Bonferroni. All data are presented as mean ± SEM. * $p < 0.05$, * * $p < 0.005$, * ** $p < 0.001$, * *** * $p < 0.0001$.

DMD patients and significantly affects participation in life (Hendriksen and Vles, 2008; Ricotti et al., 2016). Our future research will test the effects of intrathecal injections of exon 53 skipping drugs, such as Viltolarsen (Clemens et al., 2020; Komaki et al., 2018) and Golodirsen (Frank et al., 2020; Scaglioni et al., 2021), on ASD-like symptoms in DMD.

Author contributions

Y.H., H.K., K.S., Y.F., and X.D. participated in the execution and analysis of experiments. Y.H., H.K., K.S., K.Y., K.H., M.I., M.H., M.Y., T. A., H.S., S.T., K.I., N.I., F.M., M.S., and Y.A. interpreted the results. T.A., S.T., M.S., and Y.A. contributed to critical resources and reagents. Y.H., H.K., F.M., M.S., and Y.A. designed the experiments and wrote the paper. All authors edited and approved the manuscript.

Conflict of interest

The authors declare that they have no conflict of interest.

Acknowledgements

This research was supported by the Intramural Research Grant (Grant number 2-6, 30-5) for National Center of Neurology and Psychiatry (NCNP), the Japan Agency for Medical Research and Development (Grant number 20lm0203086h0002), Grants-in-Aid for Scientific Research (KAKENHI) (Grant number 19K18381 and 19H03776), Grant-in-Aid for Japan Society for the Promotion of Science (JSPS) Research Fellow (Grant number JP21J10198), and Brain involvement in dystrophinopathies (BIND) consortium (H2020 project grant 847826-).

We thank H. Takizawa, Y. Mizobe and M. Shiratori for assistance with western blot; R. Terada for assistance with RT-PCR and culture sample preparation; Y. Ookubo and H. Fujita for assistance with DMD mouse models; and K. Minegishi, E. Takeuchi, C. Vaillend, E. Ozawa and H. Kusaka for helpful discussion and comments. We thank University of North Carolina Vector Core for giving AAV5-CaMKIIa-ChR2-EYFP and Wolfson Centre for Inherited Neuromuscular Disease (CIND) for giving MANDRA1 antibody.

Appendix A. Supporting information

Supplementary data associated with this article can be found in the online version at doi:10.1016/j.pneurobio.2022.102288.

References

Alter, J., Lou, F., Rabinowitz, A., Yin, H., Rosenfeld, J., Wilton, S.D., Partridge, T.A., Lu, Q.L., 2006a. Systemic delivery of morpholino oligonucleotide restores dystrophin expression bodywide and improves dystrophic pathology. Nat. Med. 12, 175–177.

Alter, J., Lou, F., Rabinowitz, A., Yin, H., Rosenfeld, J., Wilton, S.D., Partridge, T.A., Lu, Q.L., 2006b. Systemic delivery of morpholino oligonucleotide restores dystrophin expression bodywide and improves dystrophic pathology. Nat. Med. 12, 175–177.

Amaral, D.G., Schumann, C.M., Nordahl, C.W., 2008a. Neuroanatomy of autism. Trends Neurosci. 31, 137–145.

Amaral, D.G., Schumann, C.M., Nordahl, C.W., 2008b. Neuroanatomy of autism. Trends Neurosci. 31, 137–145.

Aoki, Y., Nakamura, A., Yokota, T., Saito, T., Okazawa, H., Nagata, T., Takeda, S., 2010. In-frame dystrophin following exon 51-skipping improves muscle pathology and function in the exon 52-deficient mdx mouse. Mol. Ther. 18, 1995–2005.

Aoki, Y., Nakamura, A., Yokota, T., Saito, T., Okazawa, H., Nagata, T., Takeda, S., 2010a. In-frame dystrophin following exon 51-skipping improves muscle pathology and function in the exon 52-deficient mdx mouse. Mol. Ther. 18, 1995–2005.

Araki, E., Nakamura, K., Nakao, K., Kameya, S., Kobayashi, O., Nonaka, I., Kobayashi, T., Katsuki, M., 1997a. Targeted disruption of exon 52 in the mouse dystrophin gene induced muscle degeneration similar to that observed in Duchenne muscular dystrophy. Biochem. Biophys. Res. Commun. 238, 492–497.

Araki, E., Nakamura, K., Nakao, K., Kameya, S., Kobayashi, O., Nonaka, I., Kobayashi, T., Katsuki, M., 1997b. Targeted disruption of exon 52 in the mouse dystrophin gene induced muscle degeneration similar to that observed in Duchenne muscular dystrophy. Biochem. Biophys. Res. Commun. 238, 492–497.

Aranmolate, A., Tse, N., Colognato, H., 2017a. Myelination is delayed during postnatal brain development in the mdx mouse model of Duchenne muscular dystrophy. BMC Neurosci. 18, 63.

Aranmolate, A., Tse, N., Colognato, H., 2017b. Myelination is delayed during postnatal brain development in the mdx mouse model of Duchenne muscular dystrophy. BMC Neurosci. 18, 63.

Araque, A., Carmignoto, G., Haydon, P.G., Oliet, S.H., Robitaille, R., Volterra, A., 2014a. Gliotransmitters travel in time and space. Neuron 81, 728–739.

Araque, A., Carmignoto, G., Haydon, P.G., Oliet, S.H., Robitaille, R., Volterra, A., 2014b. Gliotransmitters travel in time and space. Neuron 81, 728–739.

Bardoni, A., Felisari, G., Sironi, M., Comi, G., Lai, M., Robotti, M., Bresolin, N., 2000a. Loss of Dp140 regulatory sequences is associated with cognitive impairment in dystrophinopathies. Neuromuscul. Disord. 10, 194–199.

Bardoni, A., Felisari, G., Sironi, M., Comi, G., Lai, M., Robotti, M., Bresolin, N., 2000b. Loss of Dp140 regulatory sequences is associated with cognitive impairment in dystrophinopathies. Neuromuscul. Disord. 10, 194–199.

Baron-Cohen, S., Ring, H.A., Bullmore, E.T., Wheelwright, S., Ashwin, C., Williams, S.C., 2000. The amygdala theory of autism. Neurosci. Biobehav. Rev. 24, 355–364.

Baron-Cohen, S., Ring, H.A., Bullmore, E.T., Wheelwright, S., Ashwin, C., Williams, S.C., 2000a. The amygdala theory of autism. Neurosci. Biobehav. Rev. 24, 355–364.

Benson, M.A., Newey, S.E., Martin-Rendon, E., Hawkes, R., Blake, D.J., 2001. Dysbindin, a novel coiled-coil-containing protein that interacts with the dystrobrevins in muscle and brain. J. Biol. Chem. 276, 24232–24241.

Berg, E.L., Copping, N.A., Rivera, J.K., Pride, M.C., Careaga, M., Bauman, M.D., Berman, R.F., Lein, P.J., Harony-Nicolas, H., Buxbaum, J.D., Ellegood, J., Lerch, J.P., Wöhr, M., Silverman, J.L., 2018. Developmental social communication deficits in the Shank3 rat model of phelan-mcdermid syndrome and autism spectrum disorder. Autism Res. 11, 587–601.

Bezzi, P., Gundersen, V., Galbete, J.L., Seifert, G., Steinhäuser, C., Pilati, E., Volterra, A., 2004. Astrocytes contain a vesicular compartment that is competent for regulated exocytosis of glutamate. Nat. Neurosci. 7, 613–620.

Blake, D.J., Nawrotzki, R., Loh, N.Y., Górecki, D.C., Davies, K.E., 1998. beta-dystrobrevin, a member of the dystrophin-related protein family. Proc. Natl. Acad. Sci. U.S.A. 95, 241–246.

Blake, D.J., Hawkes, R., Benson, M.A., Beesley, P.W., 1999. Different dystrophin-like complexes are expressed in neurons and glia. J. Cell Biol. 147, 645–658.

Bresolin, N., Castelli, E., Comi, G.P., Felisari, G., Bardoni, A., Perani, D., Grassi, F., Turconi, A., Mazzucchelli, F., Gallotti, D., et al., 1994. Cognitive impairment in Duchenne muscular dystrophy. Neuromuscul. Disord. 4, 359–369.

Caudal, D., François, V., Lafoux, A., Ledevin, M., Anegon, I., Le Guiner, C., Larcher, T., Huchet, C., 2020. Characterization of brain dystrophins absence and impact in dystrophin-deficient Dmdmdx rat model. PLoS One 15, e0230083.

Chamova, T., Guergueltcheva, V., Raycheva, M., Todorov, T., Genova, J., Bichev, S., Bojinova, V., Mitev, V., Tournev, I., Todorova, A., 2013. Association between loss of dp140 and cognitive impairment in duchenne and becker dystrophies. Balk. J. Med. Genet. 16, 21–30.

Chao, H.T., Chen, H., Samaco, R.C., Xue, M., Chahrour, M., Yoo, J., Neul, J.L., Gong, S., Lu, H.C., Heintz, N., Ekker, M., Rubenstein, J.L., Noebels, J.L., Rosenmund, C., Zoghbi, H.Y., 2010. Dysfunction in GABA signalling mediates autism-like stereotypies and Rett syndrome phenotypes. Nature 468, 263–269.

Chaussenot, R., Amar, M., Fossier, P., Vaillend, C., 2019. Dp71-dystrophin deficiency alters prefrontal cortex excitation-inhibition balance and executive functions. Mol. Neurobiol. 56, 2670–2684.

Chelly, J., Kaplan, J.C., Maire, P., Gautron, S., Kahn, A., 1988. Transcription of the dystrophin gene in human muscle and non-muscle tissue. Nature 333, 858–860.

Clemens, P.R., Rao, V.K., Connolly, A.M., Harper, A.D., Mah, J.K., Smith, E.C., McDonald, C.M., Zaidman, C.M., Morgenroth, L.P., Osaki, H., Satou, Y., Yamashita, T., Hoffman, E.P., 2020. Safety, tolerability, and efficacy of viltolarsen in boys with duchenne muscular dystrophy amenable to exon 53 skipping: a phase 2 randomized clinical trial. JAMA Neurol. 77, 982–991.

De Camilli, P., Cameron, R., Greengard, P., 1983. Synapsin I (protein I), a nerve terminal-specific phosphoprotein. I. Its general distribution in synapses of the central and peripheral nervous system demonstrated by immunofluorescence in frozen and plastic sections. J. Cell Biol. 96, 1337–1354.

Doorenweerd, N., Straathof, C.S., Dumas, E.M., Spitali, P., Ginjaar, I.B., Wokke, B.H., Schrans, D.G., van den Bergen, J.C., van Zwet, E.W., Webb, A., van Buchem, M.A., Verschuuren, J.J., Hendriksen, J.G., Niks, E.H., Kan, H.E., 2014. Reduced cerebral gray matter and altered white matter in boys with Duchenne muscular dystrophy. Ann. Neurol. 76, 403–411.

Doorenweerd, N., Mahfouz, A., van Putten, M., Kaliyaperumal, R., PAC, T.H., Hendriksen, J.G.M., Aartsma-Rus, A.M., Verschuuren, J., Niks, E.H., Reinders, M.J. T., Kan, H.E., Lelieveldt, B.P.F., 2017. Timing and localization of human dystrophin isoform expression provide insights into the cognitive phenotype of Duchenne muscular dystrophy. Sci. Rep. 7, 12575.

Dunah, A.W., Standaert, D.G., 2001. Dopamine D1 receptor-dependent trafficking of striatal NMDA glutamate receptors to the postsynaptic membrane. J. Neurosci. 21, 5546–5558.

Felisari, G., Martinelli Boneschi, F., Bardoni, A., Sironi, M., Comi, G.P., Robotti, M., Turconi, A.C., Lai, M., Corrao, G., Bresolin, N., 2000. Loss of Dp140 dystrophin isoform and intellectual impairment in Duchenne dystrophy. Neurology 55, 559–564.

Felix-Ortiz, A.C., Burgos-Robles, A., Bhagat, N.D., Leppla, C.A., Tye, K.M., 2016. Bidirectional modulation of anxiety-related and social behaviors by amygdala projections to the medial prefrontal cortex. Neuroscience 321, 197–209.

Filippo, T.D., Parisi, L., Roccella, M., 2012. Psychological aspects in children affected by duchenne de boulogne muscular dystrophy. Ment. Illn. 4, e5.

Frank, D.E., Schnell, F.J., Akana, C., El-Husayni, S.H., Desjardins, C.A., Morgan, J., Charleston, J.S., Sardone, V., Domingos, J., Dickson, G., Straub, V., Guglieri, M., Mercuri, E., Servais, L., Muntoni, F., 2020. Increased dystrophin production with golodirsen in patients with Duchenne muscular dystrophy. Neurology 94, e2270–e2282.

Fremeau Jr., R.T., Kam, K., Qureshi, T., Johnson, J., Copenhagen, D.R., Storm-Mathisen, J., Chaudhry, F.A., Nicoll, R.A., Edwards, R.H., 2004a. Vesicular glutamate transporters 1 and 2 target to functionally distinct synaptic release sites. Science 304, 1815–1819.

Fremeau Jr., R.T., Voglmaier, S., Seal, R.P., Edwards, R.H., 2004b. VGLUTs define subsets of excitatory neurons and suggest novel roles for glutamate. Trends Neurosci. 27, 98–103.

Frésard, L., Leroux, S., Dehais, P., Servin, B., Gilbert, H., Bouchez, O., Klopp, C., Cabau, C., Vignoles, F., Feve, K., Ricros, A., Gourichon, D., Diot, C., Richard, S., Leterrier, C., Beaumont, C., Vignal, A., Minvielle, F., Pitel, F., 2012. Fine mapping of complex traits in non-model species: using next generation sequencing and advanced intercross lines in Japanese quail. BMC Genom. 13, 551.

Fujino, H., Saito, T., Matsumura, T., Shibata, S., Iwata, Y., Fujimura, H., Imura, O., 2018. Autism spectrum disorders are prevalent among patients with dystrophinopathies. Neurol. Sci. 39, 1279–1282.

Fukushima, Y., Uchida, S., Imai, H., Nakatomi, H., Kataoka, K., Saito, N., Itaka, K., 2021. Treatment of ischemic neuronal death by introducing brain-derived neurotrophic factor mRNA using polyplex nanomicelle. Biomaterials 270, 120681.

Greenberg, D.S., Schatz, Y., Levy, Z., Pizzo, P., Yaffe, D., Nudel, U., 1996. Reduced levels of dystrophin associated proteins in the brains of mice deficient for Dp71. Hum. Mol. Genet. 5, 1299–1303.

Hansel, C., 2019. Deregulation of synaptic plasticity in autism. Neurosci. Lett. 688, 58–61.

Heise, C., Schroeder, J.C., Schoen, M., Halbedl, S., Reim, D., Woelfle, S., Kreutz, M.R., Schmeisser, M.J., Boeckers, T.M., 2016. Selective Localization of Shanks to VGLUT1-Positive Excitatory Synapses in the Mouse Hippocampus. Front. Cell Neurosci. 10, 106.

Hendriksen, J.G., Vles, J.S., 2008. Neuropsychiatric disorders in males with duchenne muscular dystrophy: frequency rate of attention-deficit hyperactivity disorder (ADHD), autism spectrum disorder, and obsessive–compulsive disorder. J. Child Neurol. 23, 477–481.

Hinton, V.J., Cyrulnik, S.E., Fee, R.J., Batchelder, A., Kiefel, J.M., Goldstein, E.M., Kaufmann, P., De Vivo, D.C., 2009. Association of autistic spectrum disorders with dystrophinopathies. Pedia Neurol. 41, 339–346.

Hoffman, E.P., Brown Jr., R.H., Kunkel, L.M., 1987. Dystrophin: the protein product of the Duchenne muscular dystrophy locus. Cell 51, 919–928.

Hori, K., Yamashiro, K., Nagai, T., Shan, W., Egusa, S.F., Shimaoka, K., Kuniishi, H., Sekiguchi, M., Go, Y., Tatsumoto, S., Yamada, M., Shiraishi, R., Kanno, K., Miyashita, S., Sakamoto, A., Abe, M., Sakimura, K., Sone, M., Sohya, K., Kunugi, H., Wada, K., Yamada, M., Yamada, K., Hoshino, M., 2020. AUTS2 Regulation of Synapses for Proper Synaptic Inputs and Social Communication. iScience 23, 101183.

Huang, W.C., Chen, Y., Page, D.T., 2016. Hyperconnectivity of prefrontal cortex to amygdala projections in a mouse model of macrocephaly/autism syndrome. Nat. Commun. 7, 13421.

Huang, W.C., Zucca, A., Levy, J., Page, D.T., 2020. Social Behavior Is Modulated by Valence-Encoding mPFC-Amygdala Sub-circuitry. Cell Rep. 32, 107899.

John, A., Ng-Cordell, E., Hanna, N., Brkic, D., Baker, K., 2020. The neurodevelopmental spectrum of synaptic vesicle cycling disorders. *J Neurochem.*

Kanayama, N., Fukushima, S., Nishiyama, N., Itaka, K., Jang, W.D., Miyata, K., Yamasaki, Y., Chung, U.I., Kataoka, K., 2006. A PEG-based biocompatible block catiomer with high buffering capacity for the construction of polyplex micelles showing efficient gene transfer toward primary cells. ChemMedChem 1, 439–444.

Knuesel, I., Mastrocola, M., Zuellig, R.A., Bornhauser, B., Schaub, M.C., Fritschy, J.M., 1999. Short communication: altered synaptic clustering of GABAA receptors in mice lacking dystrophin (mdx mice). Eur. J. Neurosci. 11, 4457–4462.

Komaki, H., Nagata, T., Saito, T., Masuda, S., Takeshita, E., Sasaki, M., Tachimori, H., Nakamura, H., Aoki, Y., Takeda, S., 2018. Systemic administration of the antisense oligonucleotide NS-065/NCNP-01 for skipping of exon 53 in patients with Duchenne muscular dystrophy. Sci. Transl. Med. 10.

Komoto, J., Usui, S., Otsuki, S., Terao, A., 1984. Infantile autism and Duchenne muscular dystrophy. J. Autism Dev. Disord. 14, 191–195.

Kueh, S.L., Dempster, J., Head, S.I., Morley, J.W., 2011. Reduced postsynaptic GABAA receptor number and enhanced gaboxadol induced change in holding currents in Purkinje cells of the dystrophin-deficient mdx mouse. Neurobiol. Dis. 43, 558–564.

Kuniishi, H., Yamada, D., Wada, K., Yamada, M., Sekiguchi, M., 2020. Stress induces insertion of calcium-permeable AMPA receptors in the OFC-BLA synapse and modulates emotional behaviours in mice. Transl. Psychiatry 10, 154.

Lidov, H.G., Byers, T.J., Watkins, S.C., Kunkel, L.M., 1990. Localization of dystrophin to postsynaptic regions of central nervous system cortical neurons. Nature 348, 725–728.

Lidov, H.G., Selig, S., Kunkel, L.M., 1995. Dp140: a novel 140 kDa CNS transcript from the dystrophin locus. Hum. Mol. Genet. 4, 329–335.

Makinodan, M., Rosen, K.M., Ito, S., Corfas, G., 2012. A critical period for social experience-dependent oligodendrocyte maturation and myelination. Science 337, 1357–1360.

Miranda, R., Nudel, U., Laroche, S., Vaillend, C., 2011. Altered presynaptic ultrastructure in excitatory hippocampal synapses of mice lacking dystrophins Dp427 or Dp71. Neurobiol. Dis. 43, 134–141.

Miranda, R., Nagapin, F., Bozon, B., Laroche, S., Aubin, T., Vaillend, C., 2015. Altered social behavior and ultrasonic communication in the dystrophin-deficient mdx mouse model of Duchenne muscular dystrophy. Mol. Autism 6, 60.

Mizuno, Y., Yoshida, M., Yamamoto, H., Hirai, S., Ozawa, E., 1993. Distribution of dystrophin isoforms and dystrophin-associated proteins 43DAG (A3a) and 50DAG (A2) in various monkey tissues. J. Biochem. 114, 936–941.

Motulsky, A., 1987. Duchenne Muscular Dystrophy 2. Oxford University Press, *New York*, pp. 99–106.

Moukhles, H., Carbonetto, S., 2001. Dystroglycan contributes to the formation of multiple dystrophin-like complexes in brain. J. Neurochem. 78, 824–834.

Muntoni, F., Torelli, S., Ferlini, A., 2003. Dystrophin and mutations: one gene, several proteins, multiple phenotypes. Lancet Neurol. 2, 731–740.

Nogami, K., Maruyama, Y., Sakai-Takemura, F., Motohashi, N., Elhussieny, A., Imamura, M., Miyashita, S., Ogawa, M., Noguchi, S., Tamura, Y., Kira, J.I., Aoki, Y., Takeda, S., Miyagoe-Suzuki, Y., 2021. Pharmacological activation of SERCA ameliorates dystrophic phenotypes in dystrophin-deficient mdx mice. Hum. Mol. Genet. 30, 1006–1019.

Nonneman, D.J., Brown-Brandl, T., Jones, S.A., Wiedmann, R.T., Rohrer, G.A., 2012. A defect in dystrophin causes a novel porcine stress syndrome. BMC Genom. 13, 233.

Olmos-Serrano, J.L., Paluszkiewicz, S.M., Martin, B.S., Kaufmann, W.E., Corbin, J.G., Huntsman, M.M., 2010. Defective GABAergic neurotransmission and pharmacological rescue of neuronal hyperexcitability in the amygdala in a mouse model of fragile X syndrome. J. Neurosci. 30, 9929–9938.

Pane, M., Lombardo, M.E., Alfieri, P., D'Amico, A., Bianco, F., Vasco, G., Piccini, G., Mallardi, M., Romeo, D.M., Ricotti, V., Ferlini, A., Gualandi, F., Vicari, S., Bertini, E., Berardinelli, A., Mercuri, E., 2012. Attention deficit hyperactivity disorder and cognitive function in Duchenne muscular dystrophy: phenotype-genotype correlation. J. Pedia 161 (705–709), e701.

Patel, A.M., Wierda, K., Thorrez, L., van Putten, M., De Smedt, J., Ribeiro, L., Tricot, T., Gajjar, M., Duelen, R., Van Damme, P., De Waele, L., Goemans, N., Tanganyika-de Winter, C., Costamagna, D., Aartsma-Rus, A., van Duyvenvoorde, H., Sampaolesi, M., Buyse, G.M., Verfaillie, C.M., 2019. Dystrophin deficiency leads to dysfunctional glutamate clearance in iPSC derived astrocytes. Transl. Psychiatry 9, 200.

Peça, J., Feliciano, C., Ting, J.T., Wang, W., Wells, M.F., Venkatraman, T.N., Lascola, C. D., Fu, Z., Feng, G., 2011. Shank3 mutant mice display autistic-like behaviours and striatal dysfunction. Nature 472, 437–442.

Razzoli, M., Lindsay, A., Law, M.L., Chamberlain, C.M., Southern, W.M., Berg, M., Osborn, J., Engeland, W.C., Metzger, J.M., Ervasti, J.M., Bartolomucci, A., 2020. Social stress is lethal in the mdx model of Duchenne muscular dystrophy. EBioMedicine 55, 102700.

Ricotti, V., Mandy, W.P., Scoto, M., Pane, M., Deconinck, N., Messina, S., Mercuri, E., Skuse, D.H., Muntoni, F., 2016. Neurodevelopmental, emotional, and behavioural problems in Duchenne muscular dystrophy in relation to underlying dystrophin gene mutations. Dev. Med. Child Neurol. 58, 77–84.

Roccella, M., Pace, R., De Gregorio, M.T., 2003. Psychopathological assessment in children affected by Duchenne de Boulogne muscular dystrophy. Minerva Pedia 55 (267–273), 273-266.

Romo-Yáñez, J., Rodríguez-Martínez, G., Aragón, J., Siqueiros-Márquez, L., Herrera-Salazar, A., Velasco, I., Montanez, C., 2020. Characterization of the expression of dystrophins and dystrophin-associated proteins during embryonic neural stem/progenitor cell differentiation. Neurosci. Lett. 736, 135247.

Rubenstein, J.L., Merzenich, M.M., 2003. Model of autism: increased ratio of excitation/inhibition in key neural systems. Genes Brain Behav. 2, 255–267.

Saggu, S., Cannon, T.D., Jentsch, J.D., Lavin, A., 2013. Potential molecular mechanisms for decreased synaptic glutamate release in dysbindin-1 mutant mice. Schizophr. Res. 146, 254–263.

Scaglioni, D., Catapano, F., Ellis, M., Torelli, S., Chambers, D., Feng, L., Beck, M., Sewry, C., Monforte, M., Harriman, S., Koenig, E., Malhotra, J., Popplewell, L., Guglieri, M., Straub, V., Mercuri, E., Servais, L., Phadke, R., Morgan, J., Muntoni, F., 2021. The administration of antisense oligonucleotide golodirsen reduces pathological regeneration in patients with Duchenne muscular dystrophy. Acta Neuropathol. Commun. 9, 7.

Sekiguchi, M., Zushida, K., Yoshida, M., Maekawa, M., Kamichi, S., Yoshida, M., Sahara, Y., Yuasa, S., Takeda, S., Wada, K., 2009. A deficit of brain dystrophin impairs specific amygdala GABAergic transmission and enhances defensive behaviour in mice. Brain 132, 124–135.

Smith, S.E., Zhou, Y.D., Zhang, G., Jin, Z., Stoppel, D.C., Anderson, M.P., 2011. Increased gene dosage of Ube3a results in autism traits and decreased glutamate synaptic transmission in mice. Sci. Transl. Med. 3, 103ra197.

Tachibana, R.O., Oosugi, N., Okanoya, K., 2014. Semi-automatic classification of birdsong elements using a linear support vector machine. PLoS One 9, e92584.

Talbot, K., Cho, D.S., Ong, W.Y., Benson, M.A., Han, L.Y., Kazi, H.A., Kamins, J., Hahn, C. G., Blake, D.J., Arnold, S.E., 2006. Dysbindin-1 is a synaptic and microtubular protein that binds brain snapin. Hum. Mol. Genet. 15, 3041–3054.

Tozawa, T., Itoh, K., Yaoi, T., Tando, S., Umekage, M., Dai, H., Hosoi, H., Fushiki, S., 2012. The shortest isoform of dystrophin (Dp40) interacts with a group of presynaptic proteins to form a presumptive novel complex in the mouse brain. Mol. Neurobiol. 45, 287–297.

Uchida, S., Itaka, K., Uchida, H., Hayakawa, K., Ogata, T., Ishii, T., Fukushima, S., Osada, K., Kataoka, K., 2013. In vivo messenger RNA introduction into the central nervous system using polyplex nanomicelle. PLoS One 8, e56220.

Vaillend, C., Chaussenot, R., 2017. Relationships linking emotional, motor, cognitive and GABAergic dysfunctions in dystrophin-deficient mdx mice. Hum. Mol. Genet. 26, 1041–1055.

Waite, A., Brown, S.C., Blake, D.J., 2012. The dystrophin-glycoprotein complex in brain development and disease. Trends Neurosci. 35, 487–496.

Wicksell, R.K., Kihlgren, M., Melin, L., Eeg-Olofsson, O., 2004. Specific cognitive deficits are common in children with Duchenne muscular dystrophy. Dev. Med. Child Neurol. 46, 154–159.
Yamamoto, K., Yamada, D., Kabuta, T., Takahashi, A., Wada, K., Sekiguchi, M., 2010. Reduction of abnormal behavioral response to brief restraint by information from other mice in dystrophin-deficient mdx mice. Neuromuscul. Disord. 20, 505–511.
Yizhar, O., Fenno, L.E., Prigge, M., Schneider, F., Davidson, T.J., O'Shea, D.J., Sohal, V. S., Goshen, I., Finkelstein, J., Paz, J.T., Stehfest, K., Fudim, R., Ramakrishnan, C., Huguenard, J.R., Hegemann, P., Deisseroth, K., 2011. Neocortical excitation/inhibition balance in information processing and social dysfunction. Nature 477, 171–178.
Zucker, R.S., Regehr, W.G., 2002. Short-term synaptic plasticity. Annu. Rev. Physiol. 64, 355–405.